Cold Nuclear Matter Effects from the LHC to the EIC

R. Vogt

Nuclear and Chemical Sciences Division, Lawrence Livermore National Laboratory, Livermore, CA 94551, USA
Physics and Astronomy Department, University of California, Davis, CA 95616, USA

based on:
F. Arleo *et al.*, arXiv:2506.17554, Phys. Rev. C 113, 040501 (2026)
S. Thapa *et al.*, arXiv:2510.03456, Phys. Rev. D, in press; and in preparation
C. J. Naim *et al.*, arXiv:2603.00265, submitted to Phys. Rev. D

Figure 1: **This work was performed under the auspices of the U.S. Department of Energy by Lawrence Livermore National Laboratory under Contract DE-AC52-07NA27344 and supported by the U.S. Department of Energy, Office of Science, Office of Nuclear Physics (Nuclear Theory) under contract number DE-SC-0004014 and the HEFTY Collaboration.**

Cold Nuclear Matter Effects: from the LHC to the EIC

F. Arleo *et al.*, First Perspectives article in Phys. Rev C 113, 040501 (2026)

CFNS workshop, January 2025: https://indico.cfnssbu.physics.sunysb.edu/event/338/

White paper identified key questions and discussed how to address them

- **Current Data**
- **Leading-Twist nPDF Effects vs. Saturation**
- **Energy Loss in Cold Nuclear Matter**
- **Nuclear Absorption**
- **Other Effects**
  - **Comovers**
  - **Impact Parameter Dependence of nPDF Effects**
  - **Intrinsic Heavy Flavors**
- **Future Experiments**

Some contributions from the paper are discussed

New results for quarkonium suppression combining cold and hot QCD effects are also shown

Cold Matter Effects on Hard Probes in $p+A$ Collisions

Perturbative QCD production cross section in $p+A$ collisions

$$\sigma_{pA}^{\rm pQCD}(S,m^2) \;=\; \sum_{i,j=q,\overline{q},g}\int_{4m_Q^2/S}^1 \frac{d\tau}{\tau}\int d^2b dz d\epsilon\, dx_1\, dx_2\, \delta(x_1x_2-\tau)\delta(x'_F-x_F-\delta x_F(\epsilon))\delta(x'_F-x_1+x_2)$$
$$\times P(\epsilon)\, S_A^{\rm abs}(\vec{r},z)\, S_{\rm co}(\tau)\, f_i^p(x_1,\mu_F^2,k_T^p) F_i^A(x'_1,\mu_F^2,k_T^A,\vec{b},z)\,\widehat{\sigma}_{ij}(s,m^2,\mu_F^2,\mu_R^2)$$

Survival probability for absorption of a (proto)charmonium state in nuclear matter

$$S_A^{\rm abs}(b,z) = \exp\left\{-\int_z^\infty dz'\rho_A(b,z')\sigma_{\rm abs}(z-z')\right\}$$

$S^{\rm co}$ is the survival probability for quarkonium interactions with comovers

$P(\epsilon)$ is energy loss probability that modifies the x_F of the produced J/ψ state; k_T broadening can be combined with energy loss

Nuclear parton densities, including centrality dependence

$$F_i^A(x,Q^2,\vec{b},z) = \rho_A(s) S^i(A,x,Q^2,k_T,\vec{b},z) f_i^p(x,Q^2)\;;\quad s=\sqrt{b^2+z^2}\;;\quad \rho_A(s)=\rho_0\frac{1+\omega(s/R_A)^2}{1+\exp[(s-R_A)/d]}$$

S^i is nPDF effect on parton i; no nuclear modification, $S^i(A,x,Q^2,\vec{r},z)\equiv 1$

Intrinsic heavy flavor production is added to the pQCD cross section, calculated to NLO

$$\sigma_{pA}^{\rm tot} \;=\; \sigma_{pA}^{\rm pQCD} + \sigma_{pA}^{\rm iQ}$$

Nuclear PDF Effects vs. Saturation

.

Nuclear PDFs (Shadowing)

(Left) Nuclear deep-inelastic scattering measures quark modifications directly, gluon modification is indirect

(Right) Typical shape of nPDF modification with x; varies for charge and flavor; assumes DGLAP evolution in Q^2 of all x (dilute regime)

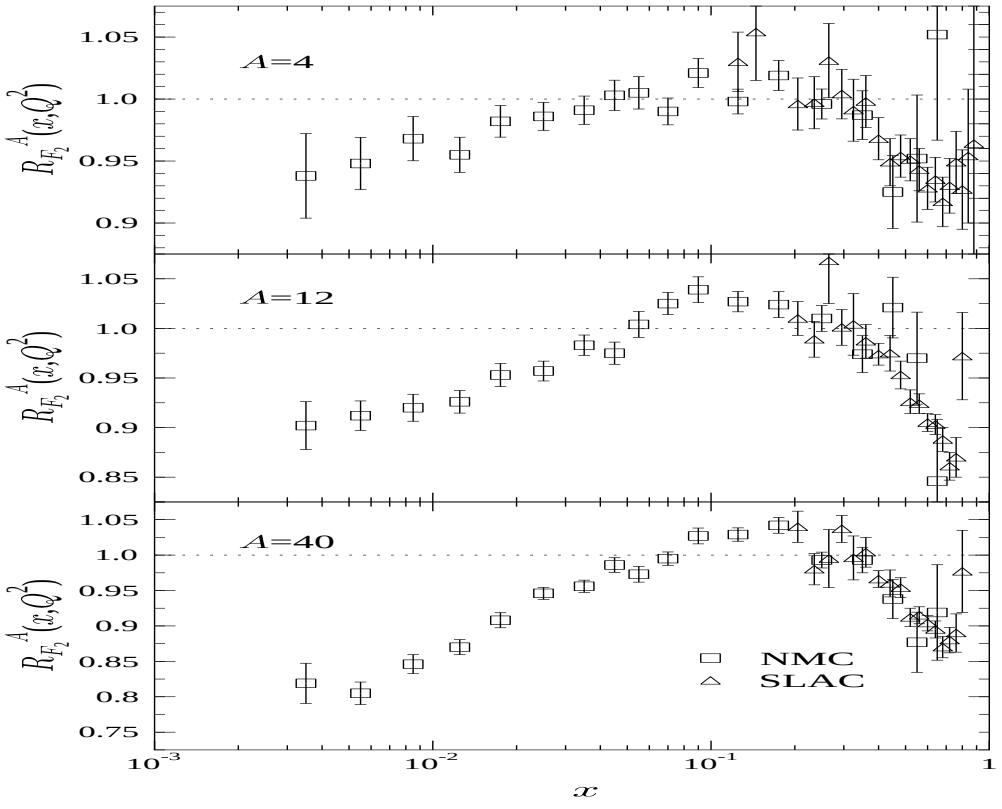

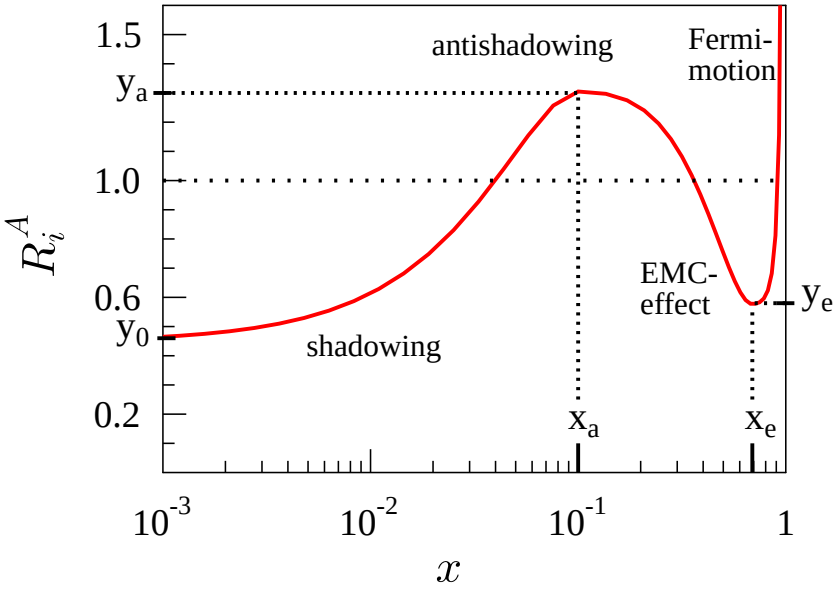

Figure 2: (Left) Ratios of charged parton densities in He, C, and Ca to D as a function of x. (Right) Illustration of typical EPPS starting fit function. [From K.J. Eskola *et al.*, JHEP **0904** (2009) 065.]

Comparison of Several nPDF Sets

Gluon distribution in a Pb nucleus for several sets: EPPS21, nCTEQ15WZ, and nNNPDF2.0 (From Eskola *et al.* EPJC 83 (2022) 413)

There are large uncertainties in the gluon ratio at $Q^2 = 10$ GeV^2 which decrease with increasing Q^2

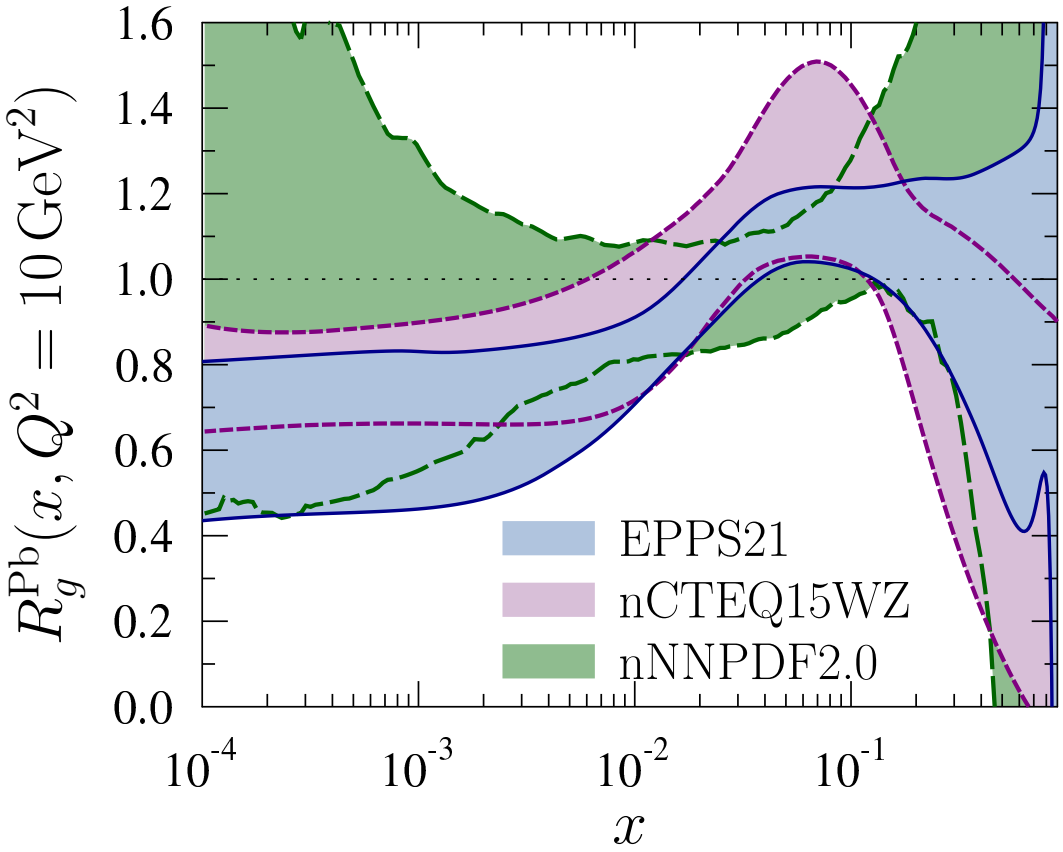

EPPS21 Comparison to Dijet Data

Comparison to CMS dijet modification (From Eskola *et al.* EPJC 83 (2022) 413)

Previous set, EPPS16, has larger uncertainties; full error includes both the nPDF uncertainties due to varying the 24 parameters as well as variations of the underlying proton parton densities

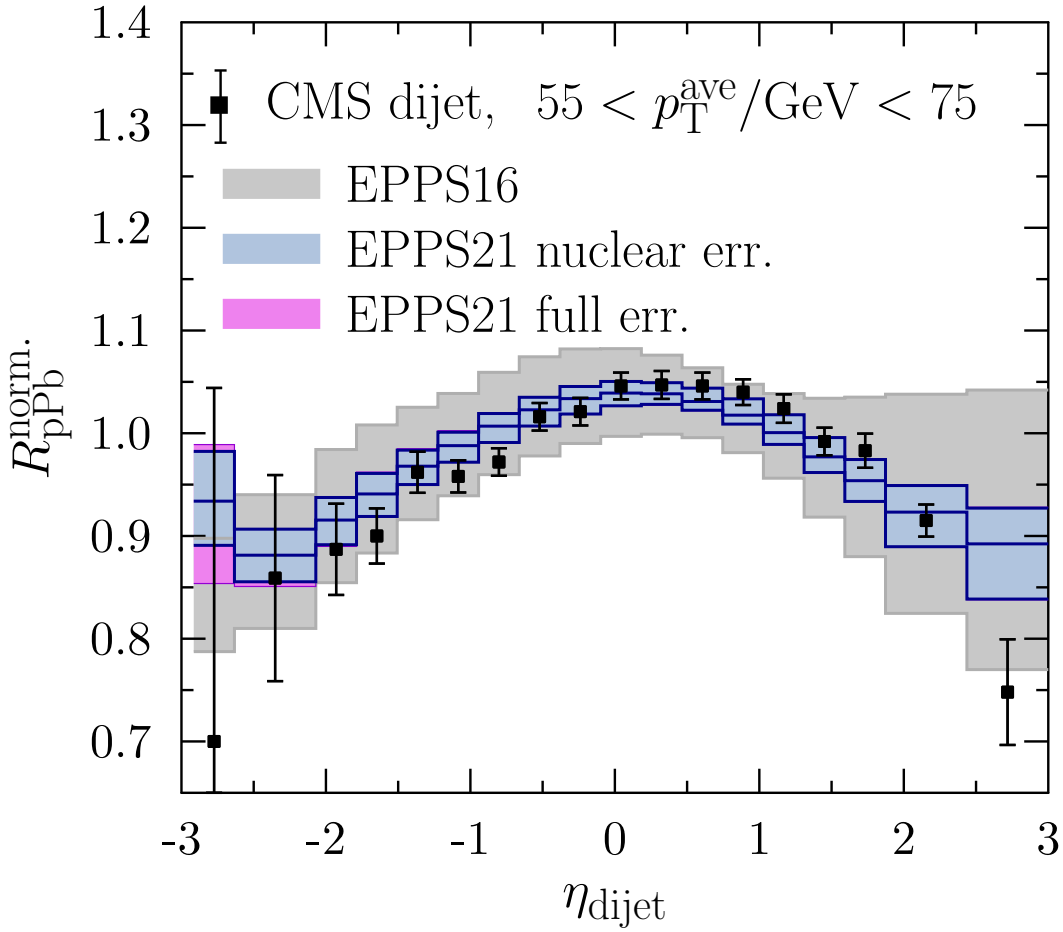

EPPS21 Comparison to D Meson Data

Comparison to LHCb D^0 modification (From Eskola *et al.* EPJC 83 (2022) 413)

Uncertainty band depends on the x range covered: at backward rapidity (left), x_2 is in the antishadowing region; at forward rapidity and small x_2, the uncertainties are larger

Note that they do not include the data for $p_T < 3$ GeV in the fits

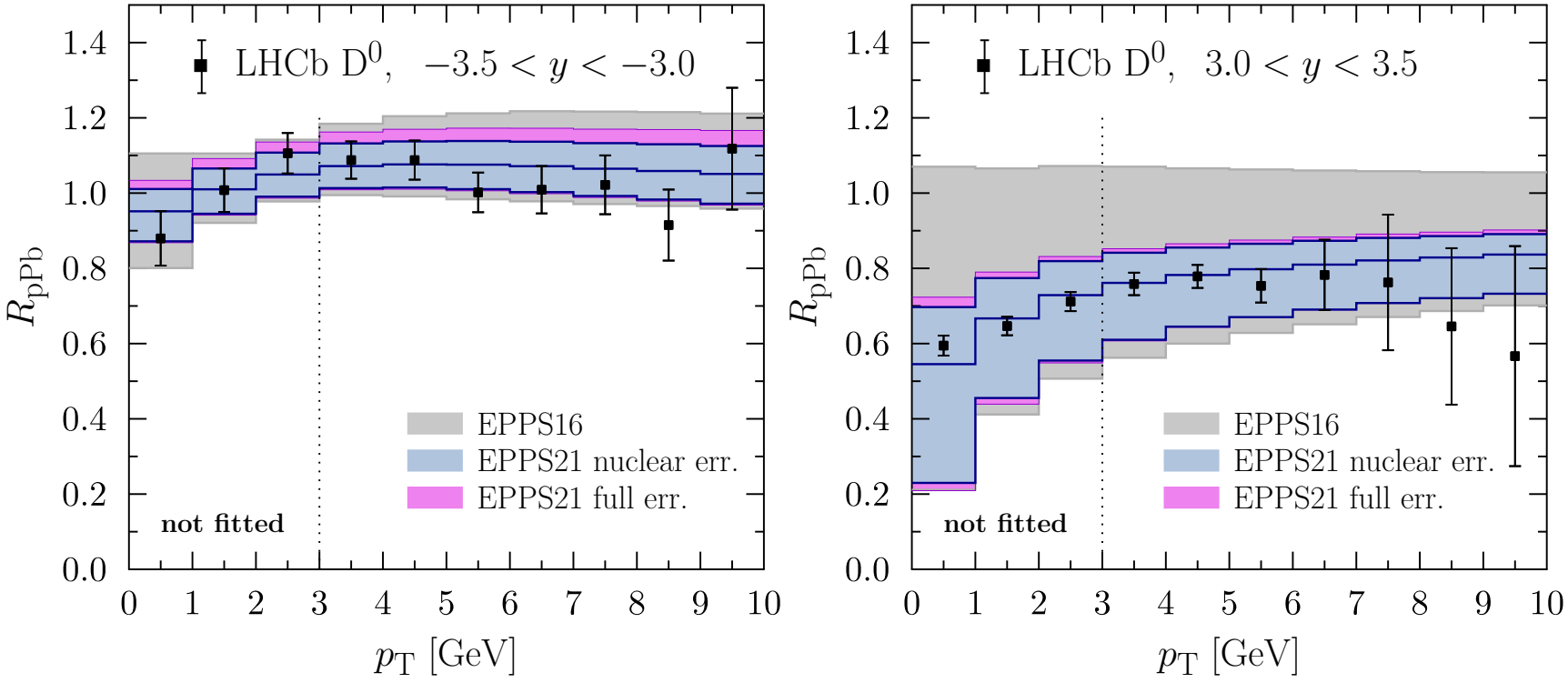

nCTEQ15 Sets

nCTEQ15 enhanced as new data became available (Figure from Phys. Rev. D 105 (2022) 114043)

Adding new data sets narrows the uncertainty bands, even at lower Q^2 (nCTEQ15 included only DIS and DY data; WZ include W and Z production at the LHC; the SIH set included semi-inclusive hadron production from RHIC; HQ includes D meson and quarkonium data (J/ψ, ψ(2S), Υ(1S))

Great improvement for the gluon (direct probe) but excludes other effects

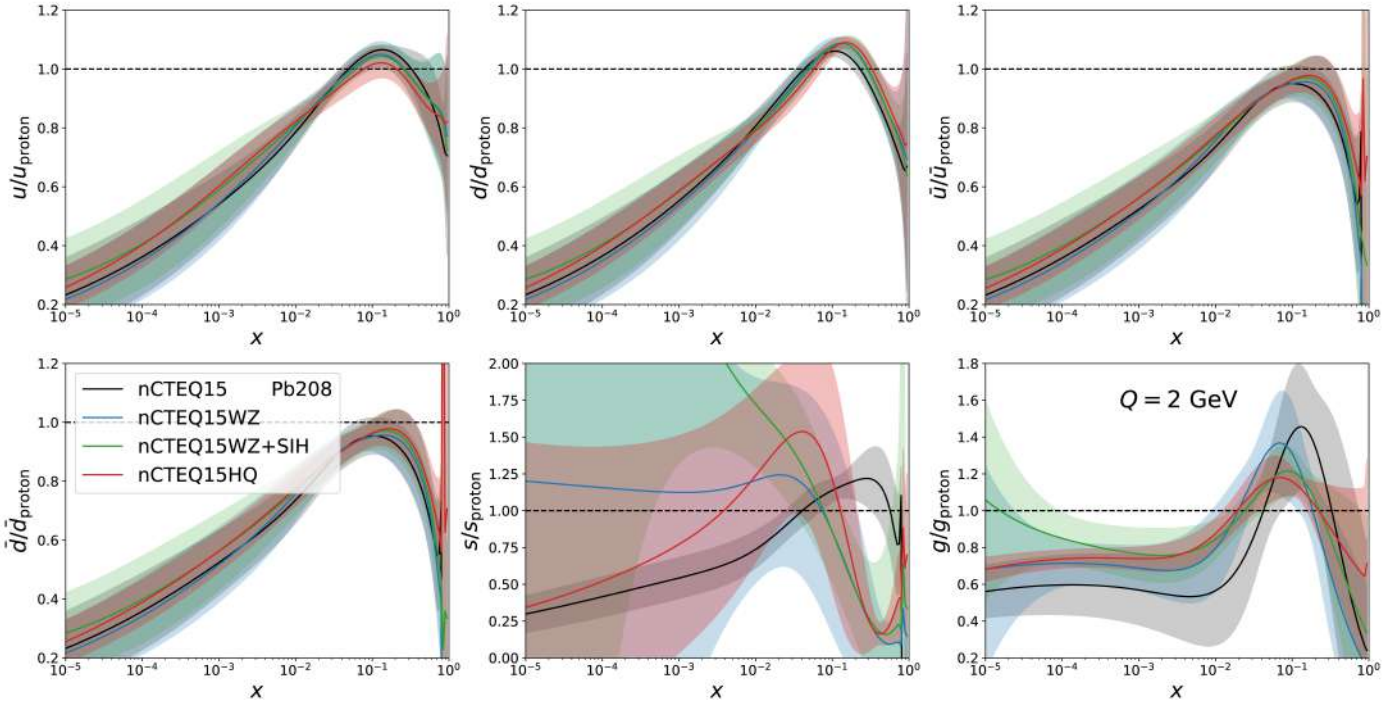

nNNPDF3.0 Sets

nNNPDF3.0 without and with including D meson data (From Eur.Phys.J. C 82 (2022) 507)

J/ψ data are not included in nNNPDF sets but the effect of adding D^0 production from LHCb is a striking improvement, particularly on the gluon distribution

Also assumes that there are no other nuclear effects than PDF modifications

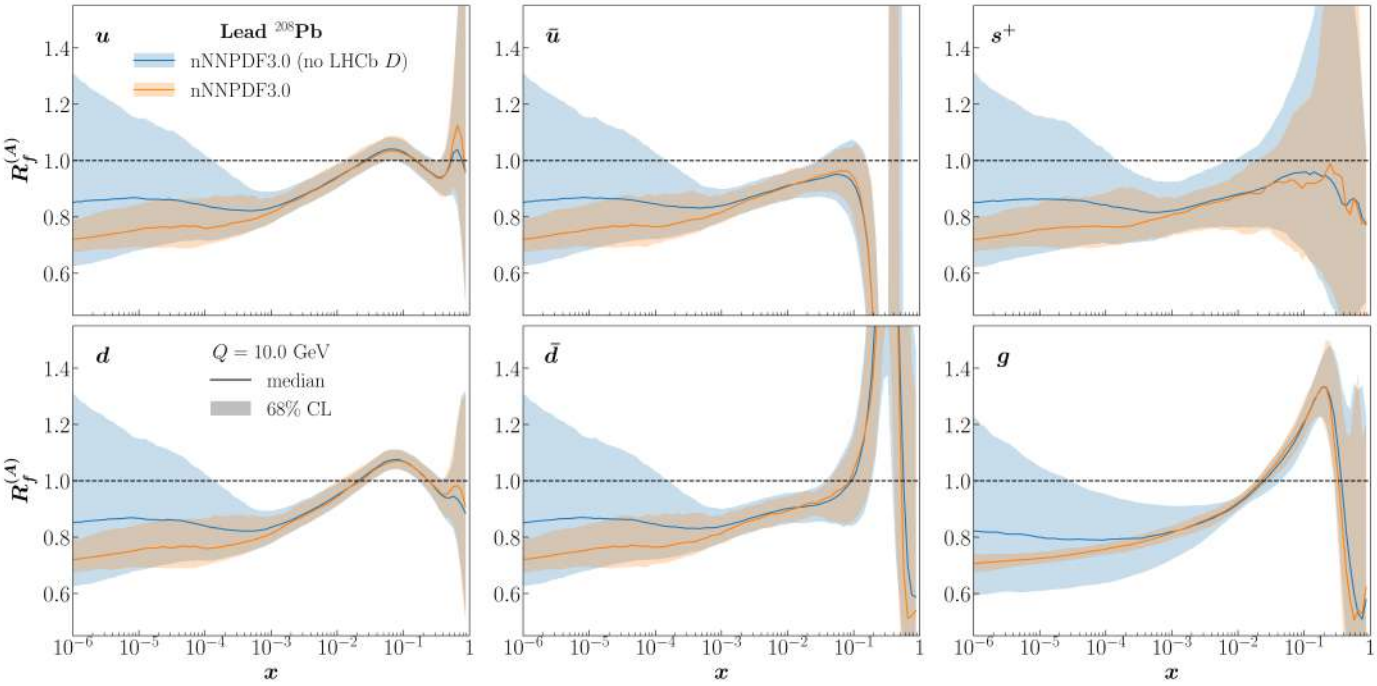

Saturation

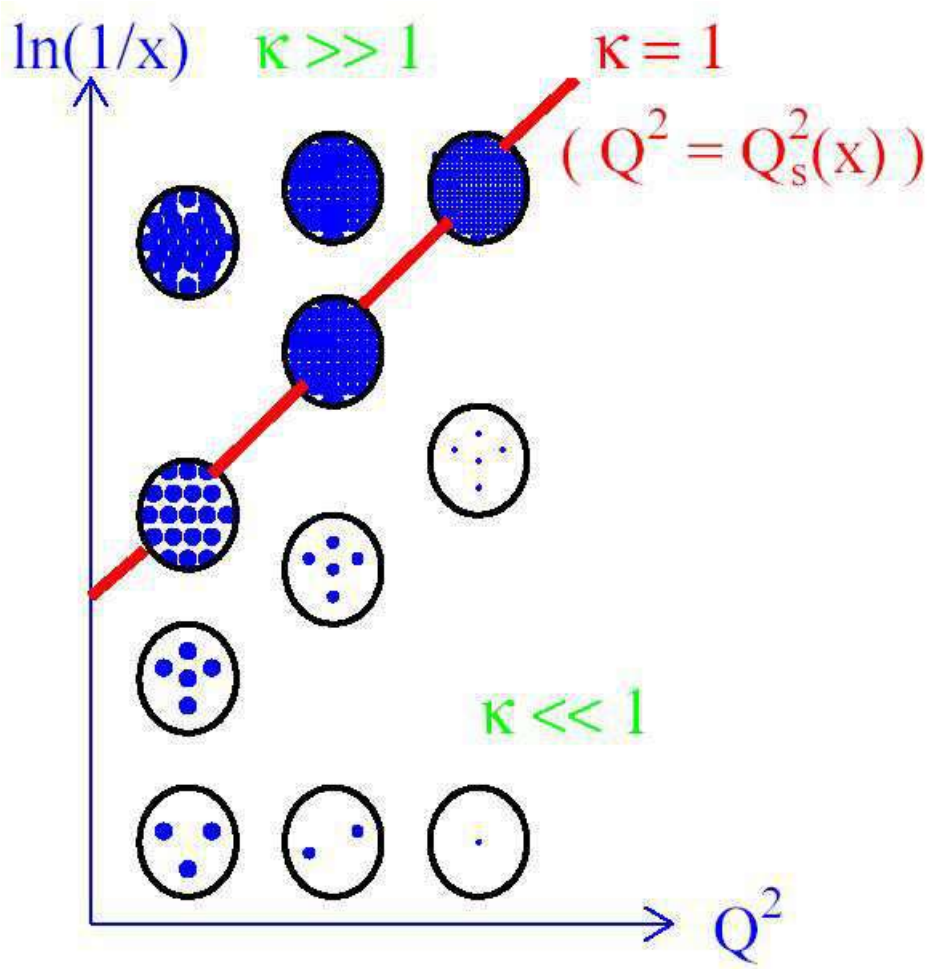

Saturation condition: when the gluon density, ρ_g, is sufficiently high, recombination of gluons $(2 \to 1)$ competes with emission of new partons $(1 \to 2)$ $\rho \sim 1/\alpha_s$

Packing factor: fraction of how much of nucleon/nuclear disk is packed with partons,
$\kappa = \sigma_{\rm dipole}/\pi R^2$, $\sigma_{\rm dipole} \propto F_2(x, Q^2)/Q^2$

Evolution is in x instead of Q^2
$Q^p_{\rm sat}$ **grows with increasing $\sqrt{s}$ and decreasing x**

In nuclei $Q^A_{\rm sat}$ increases by $A^{1/3}$

Shadowing vs. Saturation: Some comments

Saturation is inherently a low x phenomenon, it cannot address the entire x region, to do so would require matching to nPDFs at higher x

Nuclear dependence enters through the saturation scale, $Q_{\rm sat}$

nPDFs are determined by global analysis, over the entire x range, starting from a minimum scale Q_0 (1.3 GeV for the EPPS nPDFs) like the proton PDFs, and is constructed similarly using DGLAP evolution

Various groups have performed these global analyses for nPDFs: EPPS, nCTEQ, nNNPDF; previously FGS, nDS, HKN etc.; JAM Collaboration focuses also on transverse momentum and spin-dependent PDFs, including nPDFs

Data are used to adjust multiple parameters, including the mass dependence, *e.g.* EPPS21 has 24 parameters, generally leading to large uncertainties, particularly at low x for gluons, some proton PDF set is chosen as a baseline (nCTEQ based on current CTEQ, nNNPDF based on current NNPDF)

Parameterization of A dependence needed because there is not enough data on a given nucleus to cover full range of x and Q^2 (Pb comes closest)

High x region also has large uncertainties, short-range correlation studies at JLab also have mass dependence

Shadowing vs. Saturation: x and Q^2 range

(Left) DIS and Drell-Yan data cover an x and Q^2 range that does not yet reach into the saturation regime. The EIC kinematic reach will be greater and reach higher Q^2, putting the saturation regime within reach for heavy nuclei, although not penetrating far into it.

(Right) EPPS21 nPDF global analysis covered wider range of hadron and gauge boson production

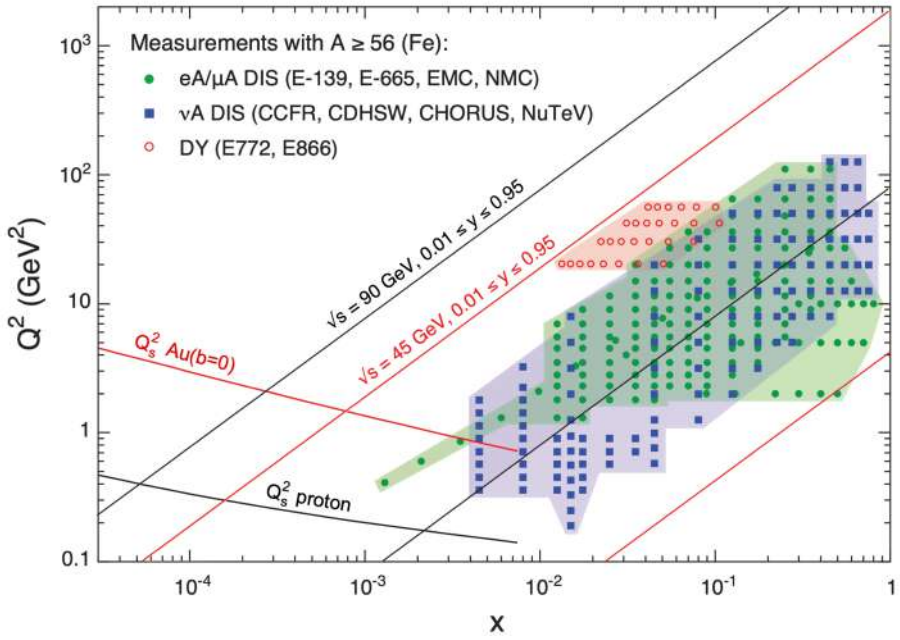

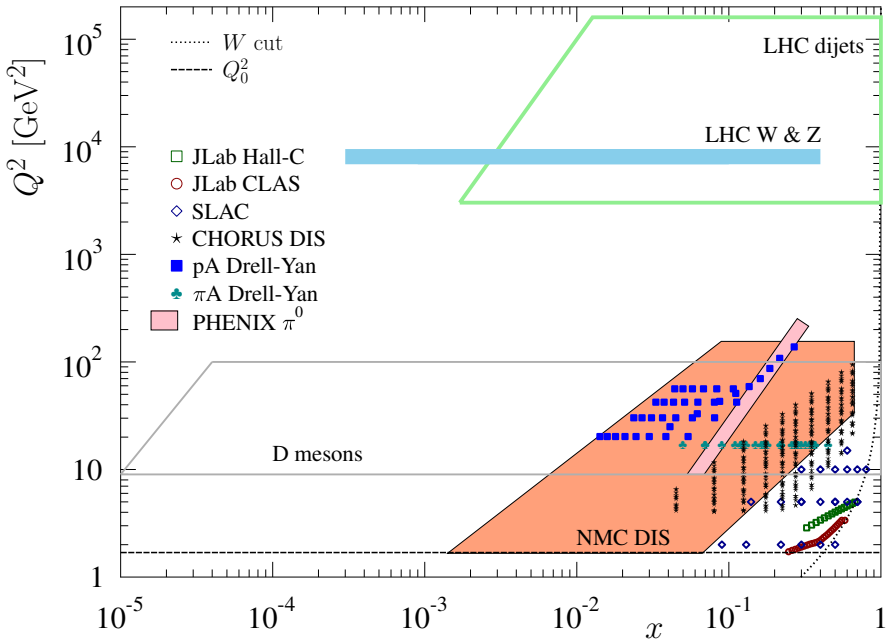

Are nPDFs the whole story?

If nuclear PDF modifications are sufficient to explain J/ψ data, then the results should be independent of $\sqrt{s_{NN}}$ and depend only on x_2

Left hand side shows J/ψ data from fixed-target energies to the LHC. The x_2 range is wide and results are very different, with experiments that reach large x_F showing the strongest modification (saturation cannot fix this)

Right hand side shows the EPPS16 gluon ratio for W/Be compared to the E866 results from $\sqrt{s_{NN}} = 38.7$ GeV. The EPPS16 results lie consistently above the data.

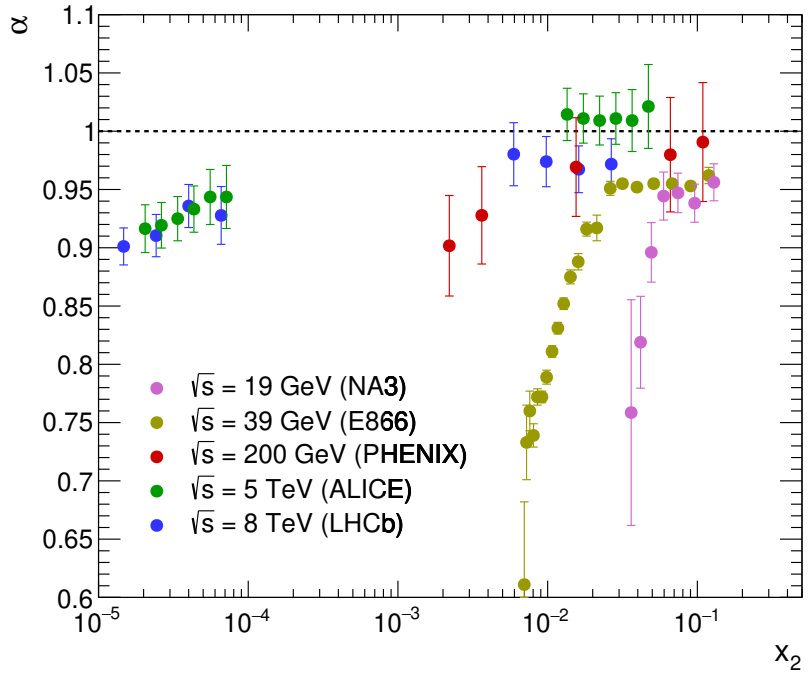

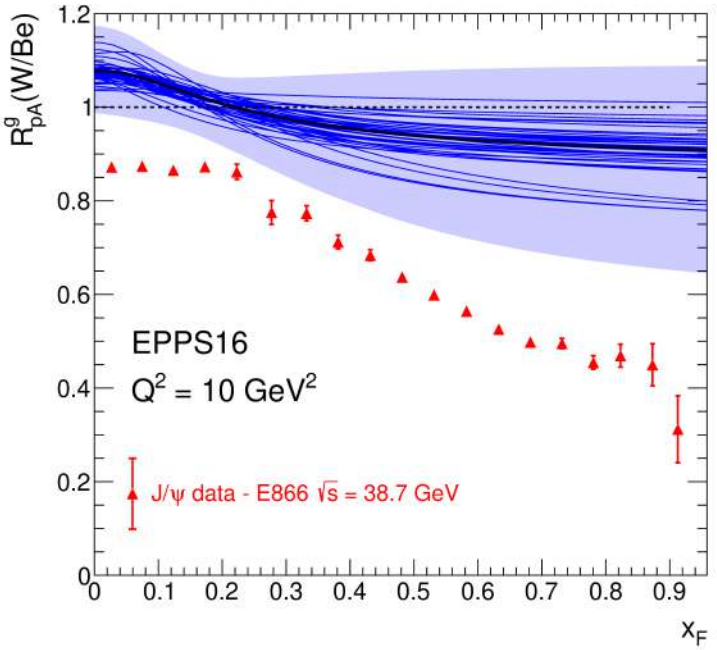

Shadowing vs. Saturation: Charged Hadron Production

At LHC energies, the CGC and nPDF predictions tend to exhibit different slopes but uncertainties make it hard to distinguish among them

CGC uncertainties include factorization and ancillary scale variations assuming that the $p + \mathrm{Pb}$ and $p + p$ cross sections are correlated

nPDF uncertainties are the variations of the parameters added in quadrature and reflect the precision of the available data

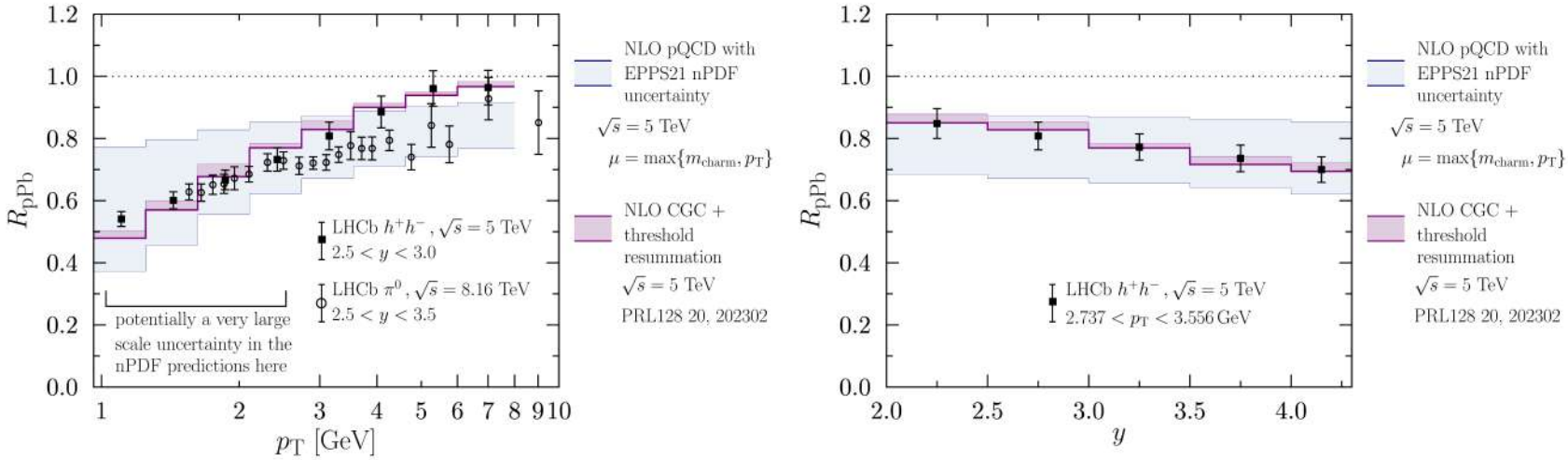

Shadowing vs. Saturation: Observables

1. **Structure function measurements in DIS – CGC and leading-twist shadowing follow different trajectories in the (x, Q^2) plane due to differences in the underlying QCD dynamics. The differences between the two types of evolution are larger for the longitudinal structure function F_L and become larger for a heavy nucleus than in a proton.**

2. **Single particle and correlated pair production in $e + A$ and $p + A$**

   - **Two-particle azimuthal correlations – disappearance of the peak at 180° as a function of azimuthal angle in the CGC. Complications: NLO correlations already decorrelate the peak and momentum broadening can remove it (CGC effects also include suppression as well as broadening, different from NLO DGLAP; heavy flavor correlations may be most relevant**
   - **Single-inclusive hadron production in $p + A$ – CGC and nPDF calculations predict different slopes of R_{pA} as a function of y and p_T; limited by typically large nPDF uncertainties**
   - **Single inclusive hadron/jet production in $e + A$ – single inclusive DIS (SIDIS) can probe saturated sea quark distributions for $p_T \sim Q_s \ll Q$; fragmentation can be a complication that can be removed by studying single-inclusive jet production**

3. **Diffractive vector meson production in $\gamma + A$ – UPCs probe low x gluon distributions, particularly for J/ψ production**

Energy Loss

.

Energy loss in medium

Based on the relative size of the formation time of a soft radiated gluon compared to the medium it travels through, the matter the gluon scatters with can be seen as incoherent scattering centers (Bethe-Heitler); partially coherent, with a group of scattering centers acts like a single radiator (LPM regime); full coherent (FCEL) where all scattering centers acts like a radiation source; and Bertsch-Gunion regime (BG-like) where initial state interactions can partially cancel radiation effects

Both longitudinal and transverse momenta are affected

All different regimes can be connected by transport coefficient $\hat{q}$

	ΔE	Observables	Systems	Facilities
Initial state LPM	$\hat{q}\,L^2\,\ln E$	Drell-Yan	$h+A$	E906, COMPASS
Final state LPM	$\hat{q}\,L^2\,\ln E$	h, jets	$e+A$	CLAS, HERMES, EIC
FCEL	$(\hat{q}\,L)^{1/2}\,(E/M_T)$	h, jets	$h+A$	SPS, FNAL, RHIC, LHC
BG-like	$f(\hat{q}\,L)L\,E$	high x_F Drell-Yan, h, jets	$h+A$	FNAL, RHIC, LHC

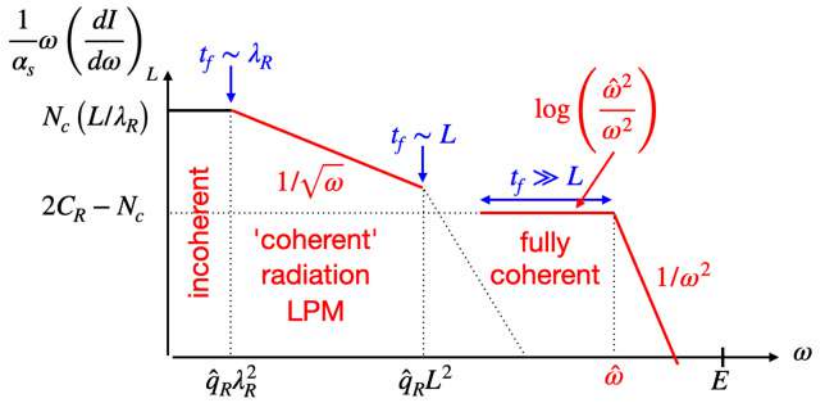

Transport Coefficient $\hat{q}$

Strength of induced gluon radiation governed by transport coefficient $\hat{q}$, related to the gluon distribution evaluated at the momentum scale $Q^2 \sim \Delta p_T^2$.

$$\hat{q} \equiv \frac{\tilde{\mu}^2}{\lambda} = \frac{4\pi^2\,\alpha_s\,C_R}{N_c^2-1}\,\rho\,xg\big(x,Q^2\big)$$

$\hat{q}$ can be determined from analyses of transverse momentum broadening, $\Delta p_T^2 = \langle p_T^2 \rangle_{hA} - \langle p_T^2 \rangle_{hp}$, related to multiple parton scattering

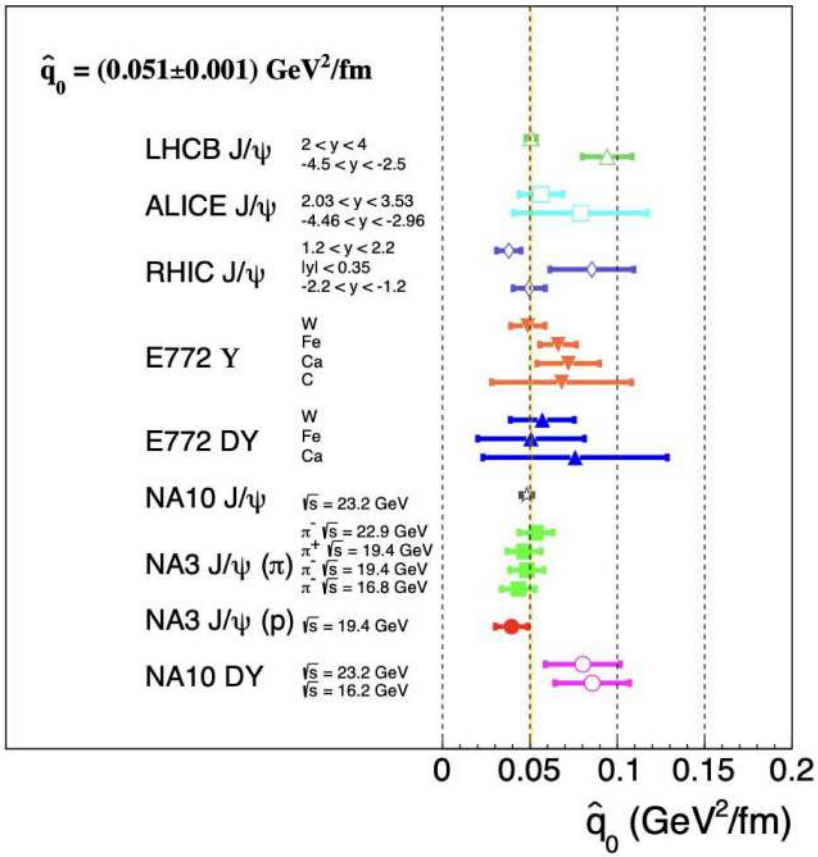

Using J/ψ Data to Pin down Nuclear Gluon PDF

The nPDF uncertainty on the low x gluon distribution can be large just based on DIS and DY data

The J/ψ is predominantly produced by gluons but is subject to other effects

Including J/ψ data can significantly reduce the uncertainties but the amount of low x shadowing depends on whether or not energy loss is taken into account

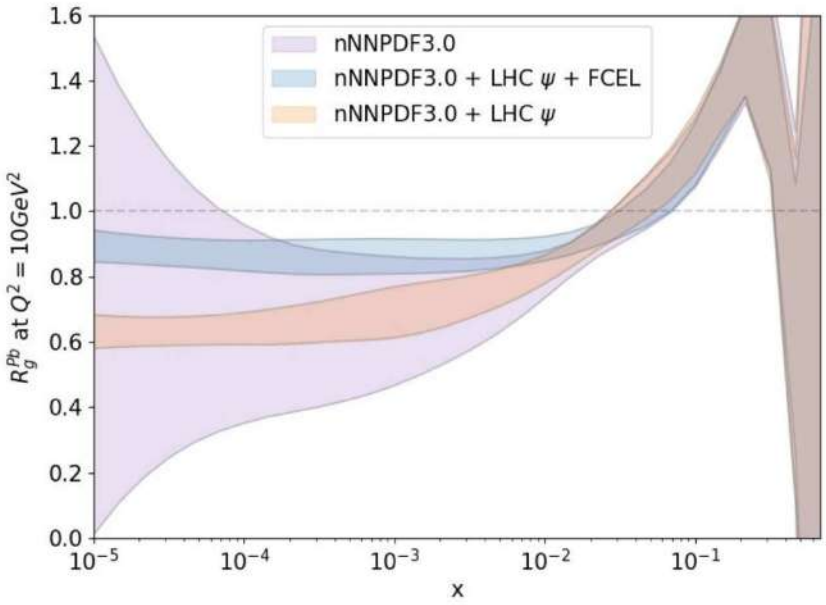

Energy Loss: Observables

1. **Drell-Yan at high x_F – well suited for studies of LPM energy loss**
2. **J/ψ production in $e+A$ and $p+A$ – FCEL depends on the color structure of the partonic process and is thus not universal; comparison of $e+A$ and $p+A$ J/ψ production could test this non-universality**

$$\begin{aligned} R_{eA}^{J/\psi}(x) &\simeq R_{eA}^{\mathbf{nPDF}}(x) \approx R_g^A(x); \\ R_{pA}^{J/\psi}(y,x_2) &\simeq R_{pA}^{\mathbf{nPDF+FCEL}}(y,x_2) \\ &\approx R_g^{\mathbf{A}}(x_2) \times R_{pA}^{\mathbf{FCEL}}(y,x_2)\,. \end{aligned}$$

3. **Direct and resolved photoproduction of forward jets and hadrons – resolved photoproduction would be sensitive to FCEL while direct photoproduction is not**
4. **$R_{pA}^{J/\psi}/R_{pA}^{\mathrm{DY}}$ at forward rapidity or large x_F – this ratio should be above unity for nPDF effects alone but smaller than unity for FCEL**
5. **$R_{pA}^{J/\psi}/R_{pA}^{\Upsilon}$ – FCEL is mass dependent, scaling like $1/m_T$, while nPDF evolution reduces the mass dependence of this effect**
6. **p_T broadening – useful for extracting $\hat{q}$ and constraining energy loss in Drell-Yan, quarkonium production, or SIDIS**
7. **Light hadrons and heavy flavors at large x_F – Bertsch-Gunion type energy loss can suppress energetic final-states at large x_F**

Absorption and Comovers: Final-State Effects

.

Absorption by Nucleons

.

Is Absorption Important for J/ψ Production?

Different methods used to extract an absorption cross section reach different conclusions about the size of $\sigma_{\rm abs}$

The absorption cross section is related to the production model (singlet, octet, or some combination) and to whether or not other CNM effects are included

Originally, absorption was a 'catch all' to cover all effects with a single, kinematics dependent parameter α, $\sigma_{pA} = \sigma_{pp} A^{\alpha}$

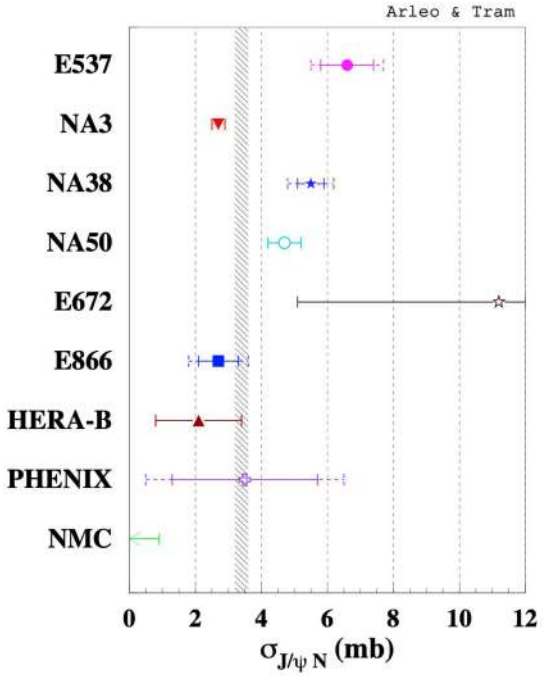

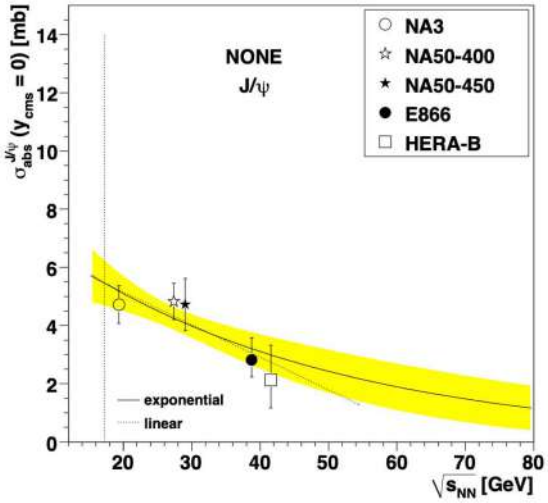

Interplay of nPDF Effects and Absorption

Depending on x values probed, shadowing can enhance or reduce absorption cross section needed to describe data

Absorption alone always gives less than linear A dependence ($\alpha < 1$)

For SPS energies, $17.3 \leq \sqrt{S} \leq 29$ GeV, rapidity range covered is in EMC and antishadowing region, $\alpha > 1$ with no absorption

Adding shadowing to absorption in the SPS energy region requires a larger absorption cross section is needed to maintain agreement with data

For $\sqrt{S} \geq 38$ GeV, x in shadowing regime, thus $\alpha < 1$ with shadowing alone in forward region, reducing needed absorption cross section to $\sigma_{\rm abs} \sim 0$ at the LHC

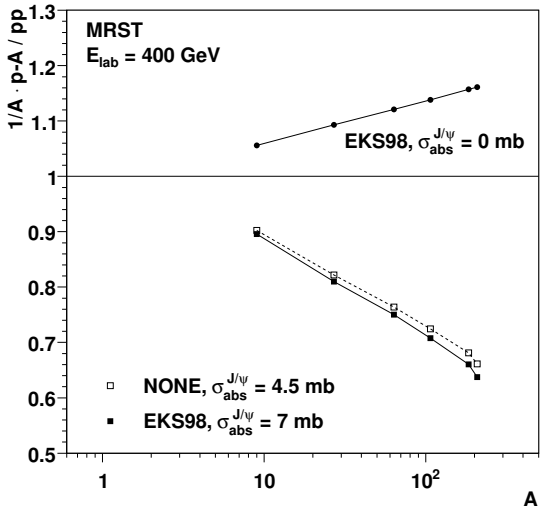

Figure 3: **(Left) Illustration of the interplay between shadowing and absorption. [C. Lourenco, H. K. Woehri and RV, JHEP 0902 (2009) 014.]**

$\sigma_{\rm abs}$ Grows with Time $c\bar{c}$ Spends Traversing Nucleus

Mid- and backward rapidity J/ψ at $\sqrt{s_{NN}} = 200$ GeV (longer $\tau = L/\gamma$) dominated by conversion of color octet $c\bar{c}$ pair to color singlet J/ψ by gluon emission

$$\sigma_{\rm abs}(\tau) = \sigma_1 \left(\frac{\sqrt{s}}{10\ GeV}\right)^{0.4} \left(\frac{r_{c\bar{c}}(\tau)}{r_{J/\psi}}\right)^2 \qquad r_{c\bar{c}}(\tau) = r_0 + v_{c\bar{c}}\tau \text{ for } r_{c\bar{c}}(\tau) < r_\psi$$

Difference at forward rapidity (shorter τ) where conversion occurs outside target

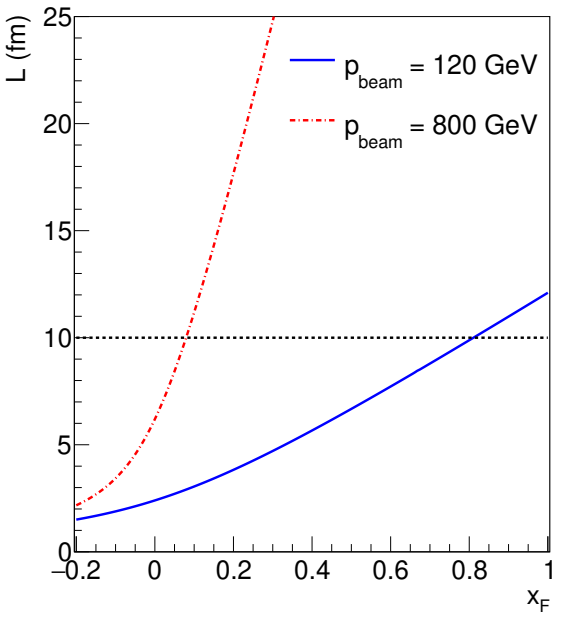

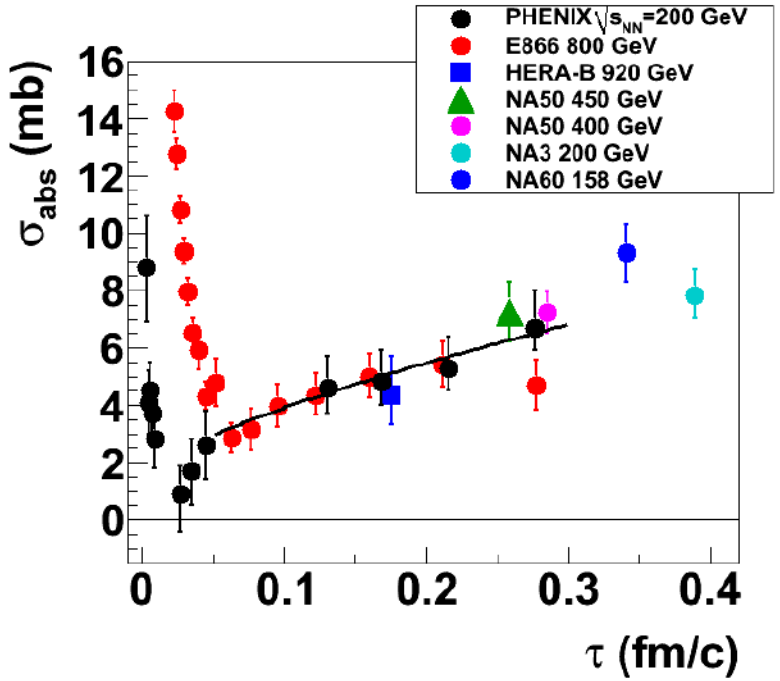

Figure 4: The effective $c\bar{c}$ breakup cross section as a function of the proper time spent in the nucleus, τ. The values were extracted from PHENIX $\sqrt{s_{NN}} = 200$ GeV d+Au data after correction for shadowing using EPS09 and from fixed-target p+A data measured by E866 at 800 GeV, by HERA-B at 920 GeV, by NA50 at 450 GeV and 400 GeV, by NA3 at 200 GeV, and by NA60 at 158 GeV. In all fixed-target cases, the EKS98 parameterization was used. The curve is calculated based on octet-to-singlet conversion inside the nucleus. [D. McGlinchey, A. D. Frawley and RV, Phys. Rev. C **87** (2013) 054910.]

Comover Interaction Model

.

Comover Interaction Model, Ferriero *et al.*

Comover interaction rate

$$\Gamma^{\mathcal{Q}}(T) = \int_{E^{Q}_{\rm thr}}^{\infty} dE^{\rm co}\, \sigma^{\mathcal{Q}}_{\rm geo} \left(1 - \frac{E^{\mathcal{Q}}_{\rm thr}}{E^{\rm co}}\right)^{n} \frac{\rho^{\rm co}}{e^{E^{\rm co}/T_{\rm eff}} - 1} \tag{1}$$

$E^{Q}_{\rm thr} = M_Q + m_{\rm co} - 2M_H$ **where** $Q = c$ **or** b, $H = D$ **or** B, $E^{\rm co} = \sqrt{p^2 + m^2_{\rm co}}$ **with** $m_{\rm co} = 0$ **for gluons and 140 MeV for pions;** ρ^0 **is the transverse density of comovers, proportional to the multiplicities;** $\sigma^0_{\rm geo} \simeq \pi r^2_Q$**; the power** n **is between 0.5 and 2 and** $T_{\rm eff} \simeq 200 - 300$ **MeV**

Dissociation of quarkonium by comover interactions as a function of time

$$\tau \frac{{\rm d}\rho^{\mathcal{Q}}}{{\rm d}\tau}\,(b,s,y) \;=\; -\sigma^{{\rm co}-\mathcal{Q}}\,\rho^{\rm co}(b,s,y)\,\rho^{\mathcal{Q}}(b,s,y)\;, \tag{2}$$

$\sigma^{{\rm co}-Q}$ **is the energy-averaged quarkonium-comover interaction cross section**

The densities of comovers and quarkonium are $\rho^{\rm co}$ **and** ρ^{Q} **respectively**

Integrating over time τ **from** τ_i **to** τ_f **gives the survival probability**

$$S^{\rm co}_{\mathcal{Q}}(b,s,y) \;=\; \exp\Big\{ -\sigma^{{\rm co}-\mathcal{Q}}\,\rho^{\rm co}(b,s,y)\,\ln\Big(\rho^{\rm co}(b,s,y)/\rho_{pp}(y)\Big)\Big\} \tag{3}$$

Shadowing is included but other cold matter effects are not

The different sizes of $\sigma^{{\rm co}-Q}$ **for** $Q = J/\psi$ **and** ψ**(2S) result in stronger comover dissociation for** ψ' **than** J/ψ

It has been shown that the A **dependence of comover interactions and nucleon absorption are effectively the same (Gavin and Vogt)**

Comover Effects on Charmonium at the LHC

$\sigma^{\mathrm{co}-Q}$ was fixed to fits to low-energy experimental data to be $\sigma^{\mathrm{co}-J/\psi} = 0.65$ mb for the J/ψ and $\sigma^{\mathrm{co}-\psi(2\mathrm{S})} = 6$ mb for the ψ(2S)

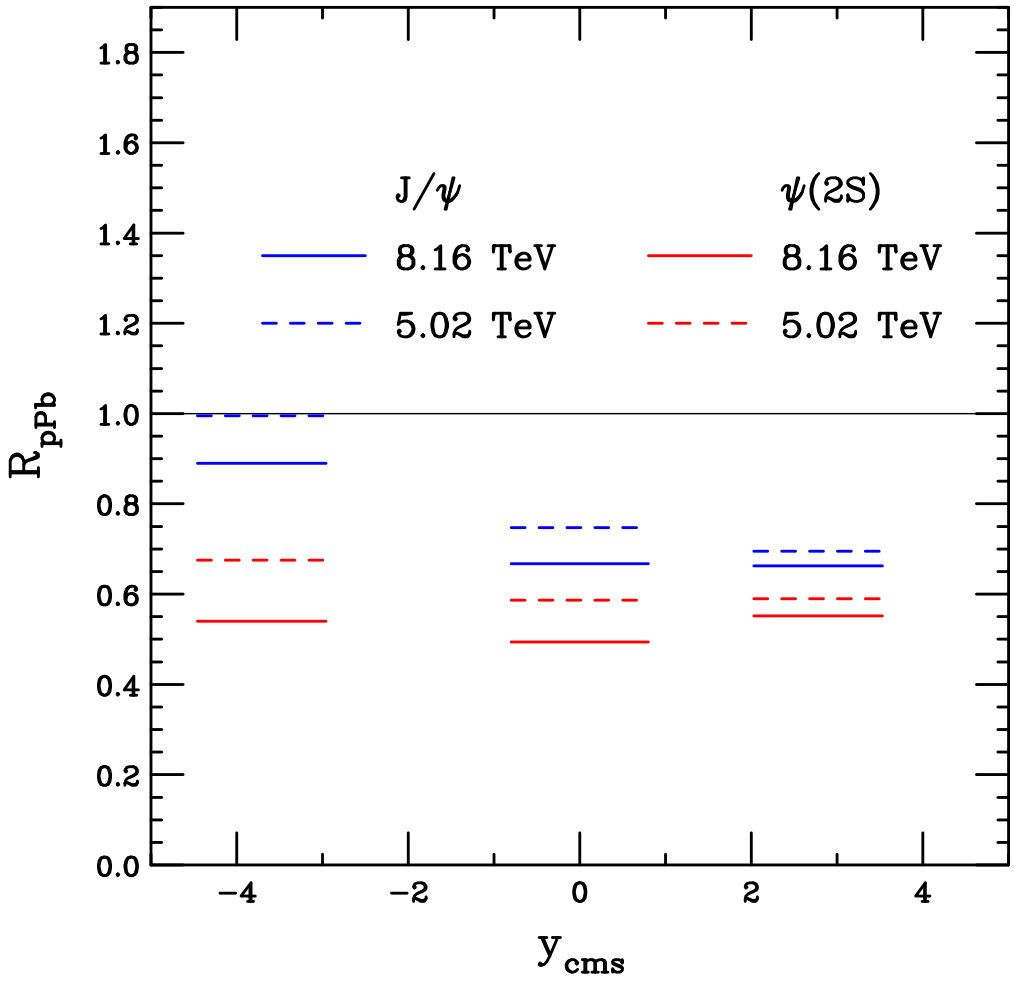

Figure 5: **The rapidity dependence of J/ψ and ψ(2S) production in the comover interaction model at 5.02 and 8.16 TeV. The EPS09 LO shadowing parameterization is also included. From Elena Ferreiro, in NPA 972 (2018) 18, arXiv:1707.09973 [hep-ph].**

Absorption and Comovers: Observables

1. **Double ratios of quarkonium states, $R^{Q\overline{Q}_i}/R^{Q\overline{Q}_j}$ – this ratio should be independent of nPDF and energy loss effects and so could isolate absorption effects for $t_{\rm form} \leq L$ where there are few comovers**
2. **Double ratios of quarkonium states, $R^{Q\overline{Q}_i}/R^{Q\overline{Q}_j}$ – in high energy collisions, $t_{\rm form} \gg L$ and absorption is negligible, this double ratio could then isolate comover effects; comparison between the double ratios for quarkonium and open heavy flavor mesons could further separate comovers from other effects**
3. **$R^{J/\psi}$ vs. R^{χ_c} – differences in the color state at production could result in different absorption cross sections**
4. **Hadron production in SIDIS in $e+p$ vs. $e+A$ – absorption effects can be isolated in regions were energy loss and nPDF effects are small**

Impact Parameter Dependent nPDF Effects

.

Impact Parameter Dependent Shadowing

.

Impact parameter dependence of shadowing first proposed in Phys. Rev. C 56, 2726 (1997)

Two parameterizations chosen, one with shadowing proportional to the nuclear density and the other proportional to the nuclear thickness at the collision point Both are normalized such that $(1/A)\int d^2bdz\rho(s)S^i(A,x,Q^2,\vec{b},z) = S^i(A,x,Q^2)$

$$S^i_{\rm WS} = S^8(A,x,Q^2,\vec{b},z) = 1 + N_{\rm WS}(S^8(A,x,Q^2)-1)\frac{\rho(\vec{b},z)}{\rho_0}$$

$$S^i_{\rm R}(A,x,Q^2,\vec{b},z) = \begin{cases} 1 + N_{\rm R}(S^i(A,x,Q^2)-1)\sqrt{1-(b/R_A)^2} & b \le R_A \\ 1 & b > R_A \end{cases} , \tag{4}$$

McGlinchey *et al.* **tried two forms for the impact parameter dependence after these original forms proved too weak for PHENIX d+Au data:**

EPS09s parameterization keeps powers $n = 1\cdots 4$ **for** A**-independent coefficients**

$$S^i(A,x,Q^2,\vec{b},z) = 1 - (1 - S^i(A,x,Q^2)\,)\left(\frac{T_A^n(b)}{a(n)}\right)$$

Impact parameter dependence assumed to be a step function with radius R **and diffuseness** d **kept as free parameters**

$$S^i(A,x,Q^2,\vec{b},z) = 1 - \left(\frac{1 - S^i(A,x,Q^2)}{a(R,d)(1+\exp((b-R)/d))}\right)$$

Centrality Dependence of CNM on J/ψ in d+Au Collisions

$$\text{Path Length Dependence } S^i_\rho(A,x,Q^2,\vec{r},z) = 1 + N_\rho(S^i(A,x,Q^2)-1)(T_A(\vec{r})/T_A(0))^n$$

$$\text{Step function Behavior } S^i_\theta(A,x,Q^2,r_T) = 1 - (\frac{1-S^i(A,x,Q^2)}{a(R,d)})/(1+\exp(r_T-R)/d)) \ ,$$

Shadowing appears to be concentrated in core of Au nucleus

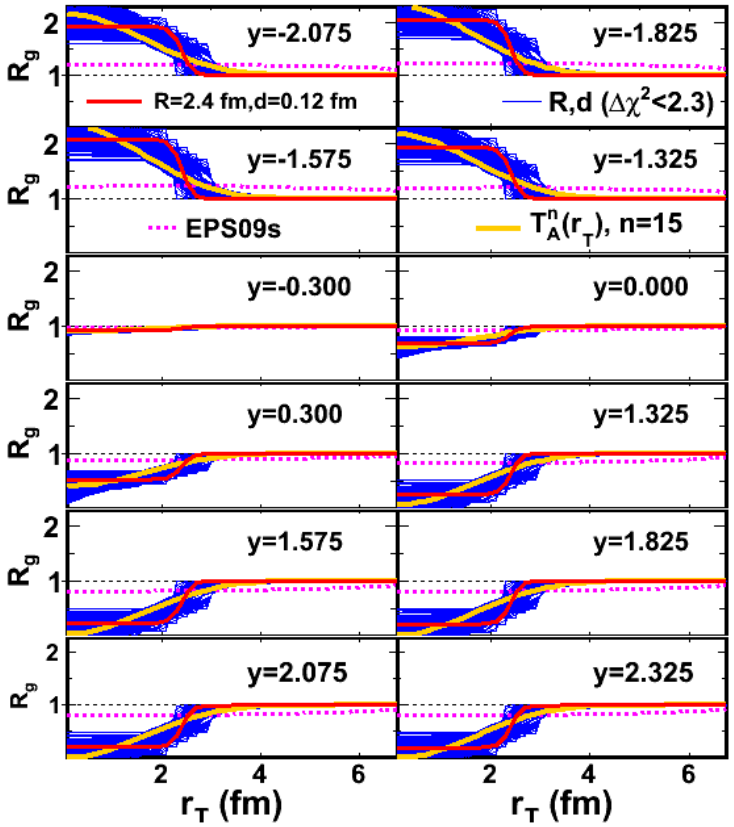

Figure 6: **Transverse radius dependence of gluon shadowing ratio R_g (based on EPS09 NLO) for the PHENIX d+Au rapidity bins. The results compare b-dependence based on path length through the nucleus, $T_A(b)$, and a sharp surface with radius and diffuseness parameters.**

Intrinsic Heavy Flavor Production

.

What are Intrinsic Heavy Flavors?

Proton wavefunction can be expanded as sum over complete basis of quark and gluon states: $|\Psi_p\rangle = \sum_m |m\rangle\, \psi_{m/p}(x_i, k_{T,i}, \lambda_i)$

$|m\rangle$ **are color singlet state fluctuations into Fock components** $|uud\rangle$, $|uudg\rangle \cdots |uudc\overline{c}\rangle$

The intrinsic Q **fluctuations can be freed by a soft interaction if the system is probed during the time** $\Delta t = 2p_{\rm lab}/M^2_{c\overline{c}}$ **that the fluctuations exist**

Dominant Fock state configurations have minimal invariant mass, $M^2 = \sum_i m^2_{T,i}/x_i$, **where** $m^2_{T,i} = k^2_{T,i} + m^2_i$ **is the squared transverse mass of parton** i **in the state; corresponds to configurations with equal rapidity constituents**

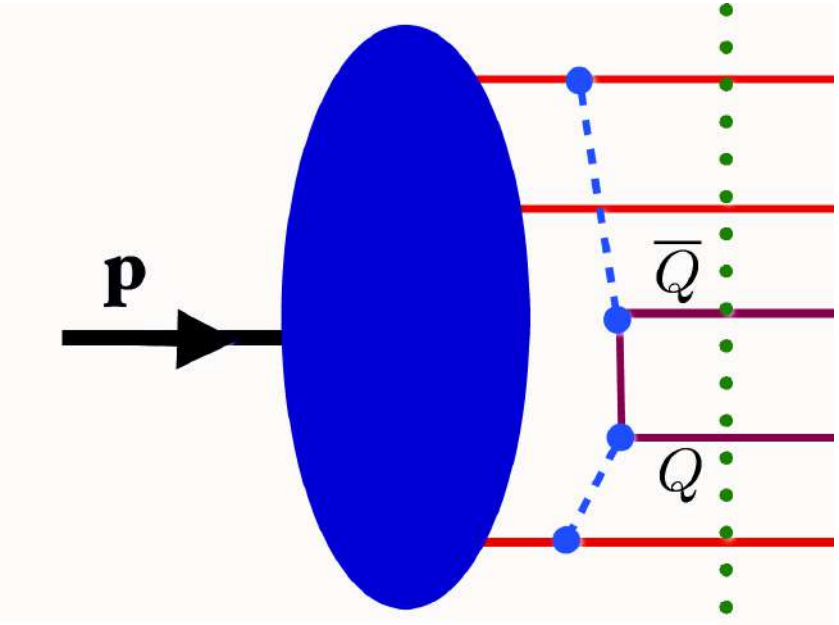

Intrinsic Charm is Long-standing Puzzle in QCD

An intrinsic charm component of the hadron wavefunction, $|uudc\bar{c}\rangle$, was first proposed by Brodsky, Hoyer, Peterson and Sakai in the 1980's

If this state is the dominant Fock component, its invariant mass is minimized, giving the charm quarks a larger fraction of the hadron momentum and leading to enhanced charm production in the forward region

A number of experimental hints have been seen, no conclusive results

- **EMC charm structure function, F_2^c, large at largest x and highest Q^2 measured in experiment**
- **Leading charm asymmetries (D^- over D^+ in $\pi^- p$ interactions, E791) consistent with intrinsic charm predictions**
- **Double J/ψ production observed at high pair x_F by NA3**
- **Forward charm production observed in many fixed-target experiments (WA82, WA89, E791, SELEX and others)**
- **Proposed explanation of high energy astrophysical neutrino rate at Ice Cube (Brodsky and Laha)**

At colliders, forward x_F pushed to very high rapidity and detection is less likely, at least for J/ψ production, lower energy, fixed-target configurations may be better for discovery measurement

LHCb: Evidence of Intrinsic Charm in $Z + c$-Jet Events

$Z+c$-jet ratio to Z+all-jet events at $\sqrt{s} = 13$ TeV is more consistent with calculations including intrinsic charm at high $y(Z)$, up to 1% intrinsic charm content

Differences between calculations without intrinsic charm (no IC) and intrinsic charm allowed calculations, either with NNPDF 3.0 including IC or CT14 with a 1% IC content, grows larger with increasing $y(Z)$

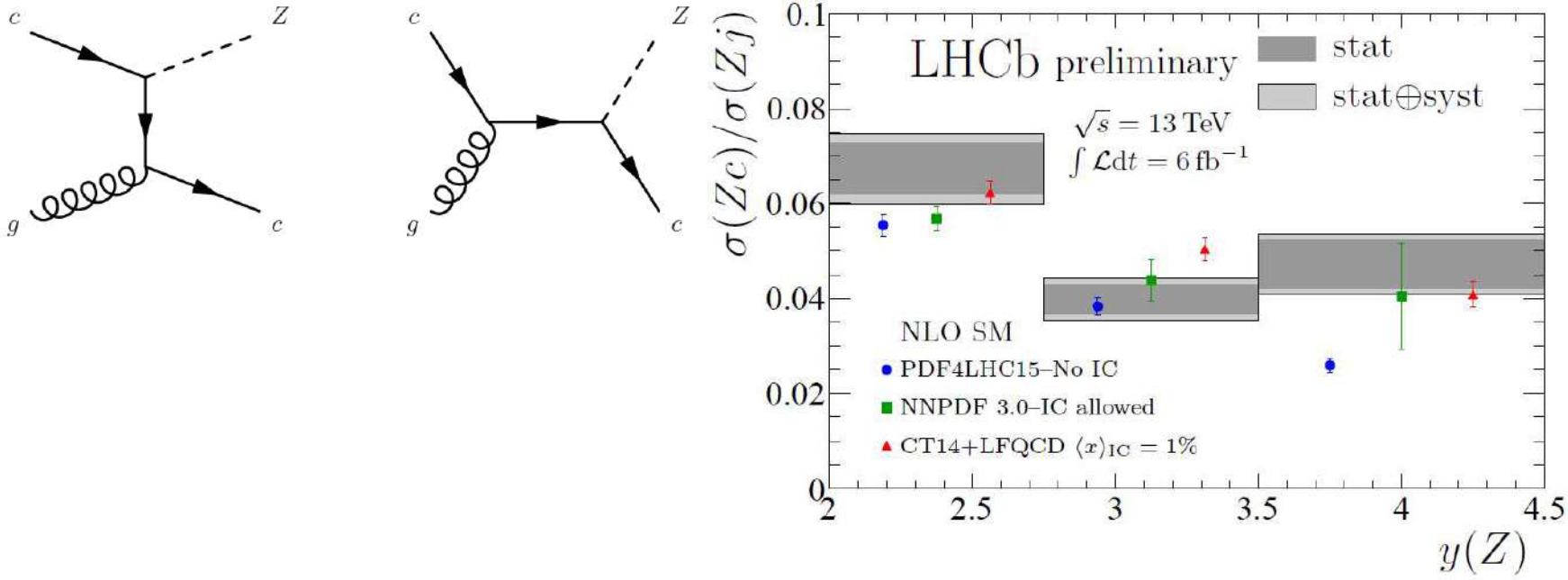

Figure 7: (Left) Leading order diagrams producing Z + c-jet events. (Right) Ratio of Z + c-jets to Z+all-jet events from LHCb. Images from https://lhcb-public.web.cern.ch/Welcome.html#IC, 27 July 2021.

Production by Intrinsic Heavy Quarks

Probability distribution of five-particle Fock state of the proton:

$$dP_{\mathrm{iQ}\,5} = P^0_{\mathrm{iQ}\,5} N_5 \int dx_1 \cdots dx_5 \int dk_{x\,1} \cdots dk_{x\,5} \int dk_{y\,1} \cdots dk_{y\,5} \frac{\delta(1-\sum_{i=1}^5 x_i)\delta(\sum_{i=1}^5 k_{x\,i})\delta(\sum_{i=1}^5 k_{y\,i})}{(m_p^2 - \sum_{i=1}^5 (\widehat{m}_i^2/x_i))^2}$$

$i = 1, 2, 3$ are u, u, d light quarks, 4 and 5 are Q and $\overline{Q}$, N_t normalizes the probability to unity and P^0_{ic} scales the normalized probability to the assumed intrinsic charm content: 0.1%, 0.31% and 1% are used to represent the range of probabilities assumed previously (based on original Brodsky *et al.* model, intrinsic bottom content would be approximately an order of magnitude smaller

The intrinsic charm cross section is determined from soft interaction scale breaking coherence of the Fock state, $\mu^2 = 0.1$ GeV^2

$$\sigma^{\mathrm{ic}}_{pp} = P_{\mathrm{ic}\,5} \sigma^{\mathrm{in}}_{pN} \frac{\mu^2}{4\widehat{m}_c^2}$$

The cross sections from intrinsic charm are then obtained by multiplying by the normalization factor for the CEM to the J/ψ

$$\sigma^{\mathrm{ic}}_{pp}(J/\psi) = F_C \sigma^{\mathrm{ic}}_{pp} \quad \sigma^{\mathrm{ic}}_{pA} = \sigma^{\mathrm{ic}}_{pp}\, A^{\beta} \quad , \beta = 0.71 \ \text{(NA3)}$$

Brodsky *et al.* Original Intrinsic Charm

Probability distribution of five-particle Fock state of the proton:

$$dP_{\mathrm{ic}\,5} = P^0_{\mathrm{ic}\,5} N_5 \int dx_1 \cdots dx_5 \int dk_{x\,1} \cdots dk_{x\,5} \int dk_{y\,1} \cdots dk_{y\,5} \frac{\delta(1-\sum_{i=1}^5 x_i)\delta(\sum_{i=1}^5 k_{x\,i})\delta(\sum_{i=1}^5 k_{y\,i})}{(m_p^2 - \sum_{i=1}^5 (\widehat{m}_i^2/x_i))^2}$$

$i = 1, 2, 3$ are u, u, d light quarks, 4 and 5 are c and $\overline{c}$, N_t normalizes the probability to unity and P^0_{ic} scales the normalized probability to the assumed intrinsic charm content: 0.1%, 0.31% and 1% are used to represent the range of probabilities assumed previously

The IC cross section is determined from soft interaction scale breaking coherence of the Fock state, $\mu^2 = 0.1$ GeV^2

$$\sigma_{\mathrm{ic}}(pp) = P_{\mathrm{ic}\,5} \sigma^{\mathrm{in}}_{pN} \frac{\mu^2}{4\widehat{m}_c^2}$$

The cross sections from intrinsic charm are then obtained by multiplying by the normalization factor for the CEM to the J/ψ while we assume direct correspondence with IC cross section for $\overline{D}^0$

$$\sigma^{\overline{D}}_{\mathrm{ic}}(pp) = \sigma_{\mathrm{ic}}(pp) \quad , \sigma^{J/\psi}_{\mathrm{ic}}(pp) = F_C \sigma_{\mathrm{ic}}(pp)$$

The A dependence is the same for both $\overline{D}$ and J/ψ

$$\sigma_{\mathrm{ic}}(pA) = \sigma_{\mathrm{ic}}(pp)\, A^{\beta}$$

where $\beta = 0.71$ for a proton beam on a nuclear target, as determined by NA3

Other Interpretations of Intrinsic Charm in PDFs

General notion of nonperturbative charm in the parton densities

Radiatively generated charm, also called "extrinsic charm", is charm parton density determined by the gluon and light quark parameters and DGLAP evolution

Several groups assessed nonperturbative contributions through general global analyses, including coherent treatment of nonzero quark masses in pQCD and experimental inputs that constrain the charm degree of freedom (e, ν data from fixed-target DIS with proton and light nuclear targets, HERA, and other data)

One of the first, by Pumplin *et al.* Compared three different scenarios:

- **Light cone formalism of Brodsky *et al.***

$$c(x) = \overline{c}(x) = Ax^2[6x(1+x)\ln x + (1-x)(1+10x+x^2)]$$

- **Meson/baryon cloud model with $c(x) \neq \overline{c}(x)$**

$$c(x) = Ax^{1.897}(1-x)^{6.095}\,, \qquad \overline{c}(x) = \overline{A}x^{2.511}(1-x)^{4.929}\,, \qquad 0 = \int_0^1 dx[c(x) - \overline{c}(x)]$$

- **Charm distribution is sea-like, similar to light flavor sea**

$$c(x) = \overline{c}(x) \propto \overline{d}(x) + \overline{u}(x)$$

The NNPDF collaboration has used machine learning with more unstructured parameterizations to look for evidence of large x charm content

PDF Analyses Including Intrinsic Charm

- **Hoffman and Moore calculated intrinsic charm at NLO for EMC only (1983), include mass effects and scale evolution**
- **Harris, Smith and RV made NLO calculation of extrinsic and intrinsic charm at NLO, 1990, found approximate $(0.86 \pm 0.60)\%$ contribution at highest Q^2 fitting EMC data only**
- **Pumplin *et al.* made first global analysis of proton PDFs (2007) including intrinsic charm assuming BHPS and meson-cloud model ($c(x) \neq \overline{c}(x)$) shapes as well as 'sea-like' with the same shape as radiatively-generated extrinsic charm, the CTEQ6.6C sets**
- **Dulat *et al.*, based on CT10 NNLO PDFs, included DIS and hadroproduction, found $\langle x \rangle_{c+\overline{c}}(Q_0^2) \leq 0.025$ for BHPS, ≤ 0.015 for sea-like**
- **Jimenez-Delgado *et al.*, included lower energy data and more stringent tolerance than Dulat, found $\langle x \rangle_{c+\overline{c}} < 0.1\%$ at 5σ level (agree with Dulat with same tolerance)**
- **NNPDF Collaboration (Ball *et al.*) compared global analyses with "perturbative charm" (extrinsic) and "fitted charm" (intrinsic charm), concluded that charm at low x is perturbative but, at low scales and high x, the data support an intrinsic component**

NNPDF4: Evidence for Intrinsic Charm I

Parameterize the 4 flavor number scheme (4FNS) freely and fit charm in a global analysis, matching to 3FNS can be inverted to obtain the intrinsic charm component if the 3FNS contribution does not vanish, as with no intrinsic charm

Extracted 3FNS charm distribution shows a valence-like structure at large x, with a peak around $x \sim 0.4$; no radiatively generated charm in this region

Missing higher order uncertainties (MHOU) estimated by transforming from 4FNS PDF at NNLO at N^{3}LO; peak does not change but uncertainties for $x < 0.2$ become very large (light blue band is PDFU + MHOU added in quadrature)

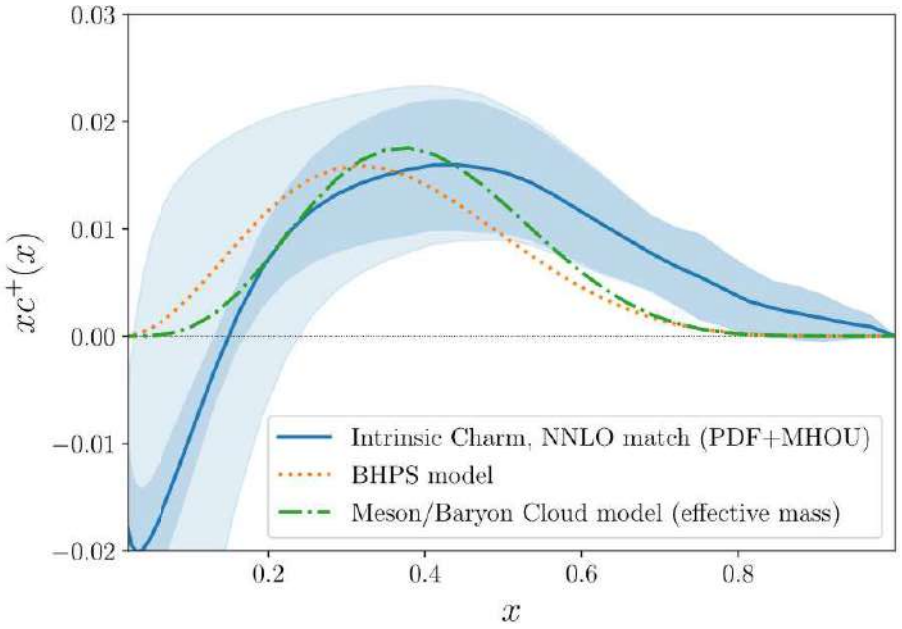

Figure 8: Dark Blue band shows the extracted intrinsic charm distribution with PDF uncertainties only, based on the NNPDF4.0 PDFs; light blue band includes MHOU; orange line is the Brodsky *et al.* distribution and the dark green line is the charm distribution from the meson/baryon cloud model. [NNPDF Collaboration, Nature **608** (2022) 483–487].

NNPDF4: Evidence for Intrinsic Charm II

NNPDF Collaboration studied the stability of their results by looking at the dependence on the datasets used in the analysis; the parameterization basis (evolution basis – linear combinations of q and $\overline{q}$ distributions – or individual PDF basis); charm quark mass dependence

The charm momentum fraction (probability for intrinsic charm) is between 0.5% and 0.8%, albeit with large combined uncertainties, particularly from the MHOU

Statistical significance reaches 3 sigma with LHCb $Z + c$-jet and EMC data are included (either and both)

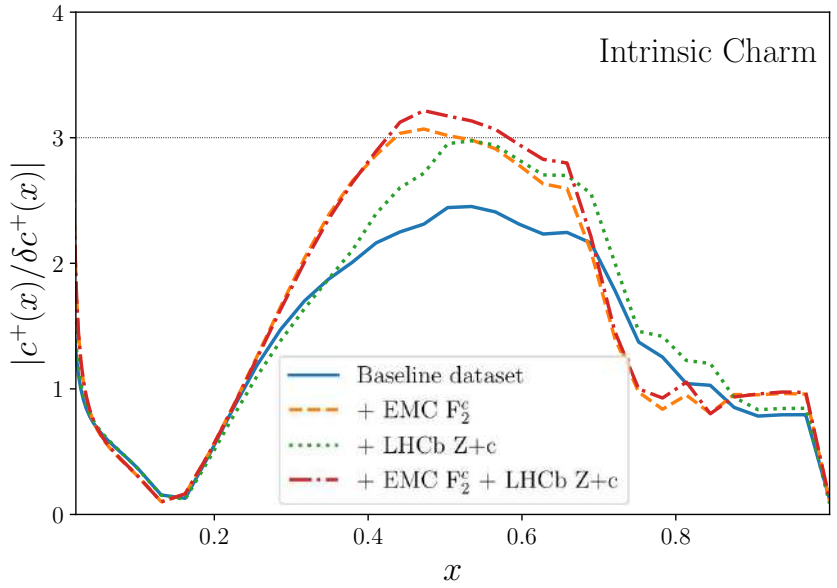

Figure 9: Statistical significance of the results for the baseline dataset (without the $Z + c$-jet and EMC data) and adding in one or both of these higher x datasets. [NNPDF Collaboration, Nature **608** (2022) 483–487.]

Counterarguments: CT18 (Guzzi *et al.*) I

Argue that fitted charm PDF that parameterizations of $xc(x)$ extracted near threshold are only approximation because they may absorb contributions unrelated to IC and that without a way to connect the fitted charm in PDF analyses to IC models it is impossible to guarantee that the resulting IC is a universal component of the proton wavefunction

Most available DIS measurements are low x and thus not very sensitive to IC; the NNLO $Z + c$-jet calculation has not been incorporated into global analyses so they claim these data are not sufficiently accurate to discriminate between IC models

Augmented CT18 with 4 variations of fitted charm and underlying IC model: BHPS (standard IC with either CT18 NNLO or CT18X NNLO) and MCM (meson cloud model with $p \equiv \overline{D}\Lambda_c$ and either confining or effective mass quark models)

All four models give low probability for intrinsic charm (related to first moment,

$$\langle x \rangle (Q_0^2) \sim 0.004 - 0.006 \tag{5}$$

Claim that NNPDF "evidence" would also equally well allow a nearly zero IC contribution with more comprehensive sampling and that their uncertainties are underestimated (they also note that otherwise the frameworks and procedures are similar for NNPDF and CT18)

Counterarguments: CT18 (Guzzi *et al.*) II

Left side shows the four variations of fitted charm used for the analysis, all peaking at higher x than perturbatively generated charm

Figures on the right show the difference in the LHCb $Z + c$-jet analysis based on whether or not the generator used with the PDFs includes parton showering or not; including showering enhances the intrinsic charm (difference between Powheg and MCFM); with MCFM and more recent PDF sets, the difference calculations do not match the data as well

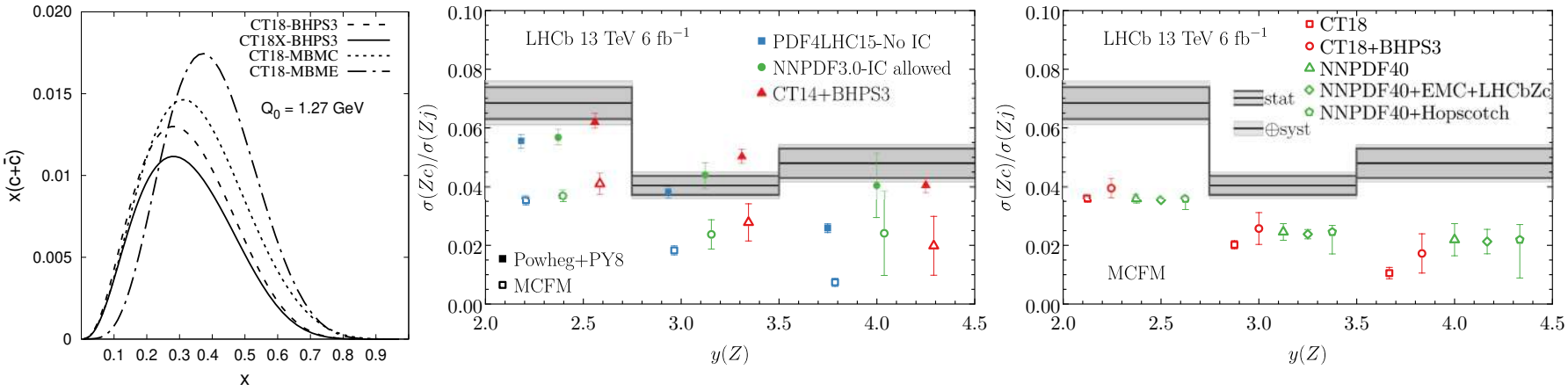

Figure 10: CT18, Guzzi *et al.*, arXiv:2211.01387.

Intrinsic Charm x_F and p_T Distributions

Peak of the J/ψ x_F distribution is forward, at low energy, intrinsic charm is

p_T distribution is harder than the pQCD distribution at low energy; at higher energies and $x_F \sim 0$, the pQCD contribution will drown the intrinsic charm contribution

The p_T distribution also depends on range of k_T integration, x_F distribution does not

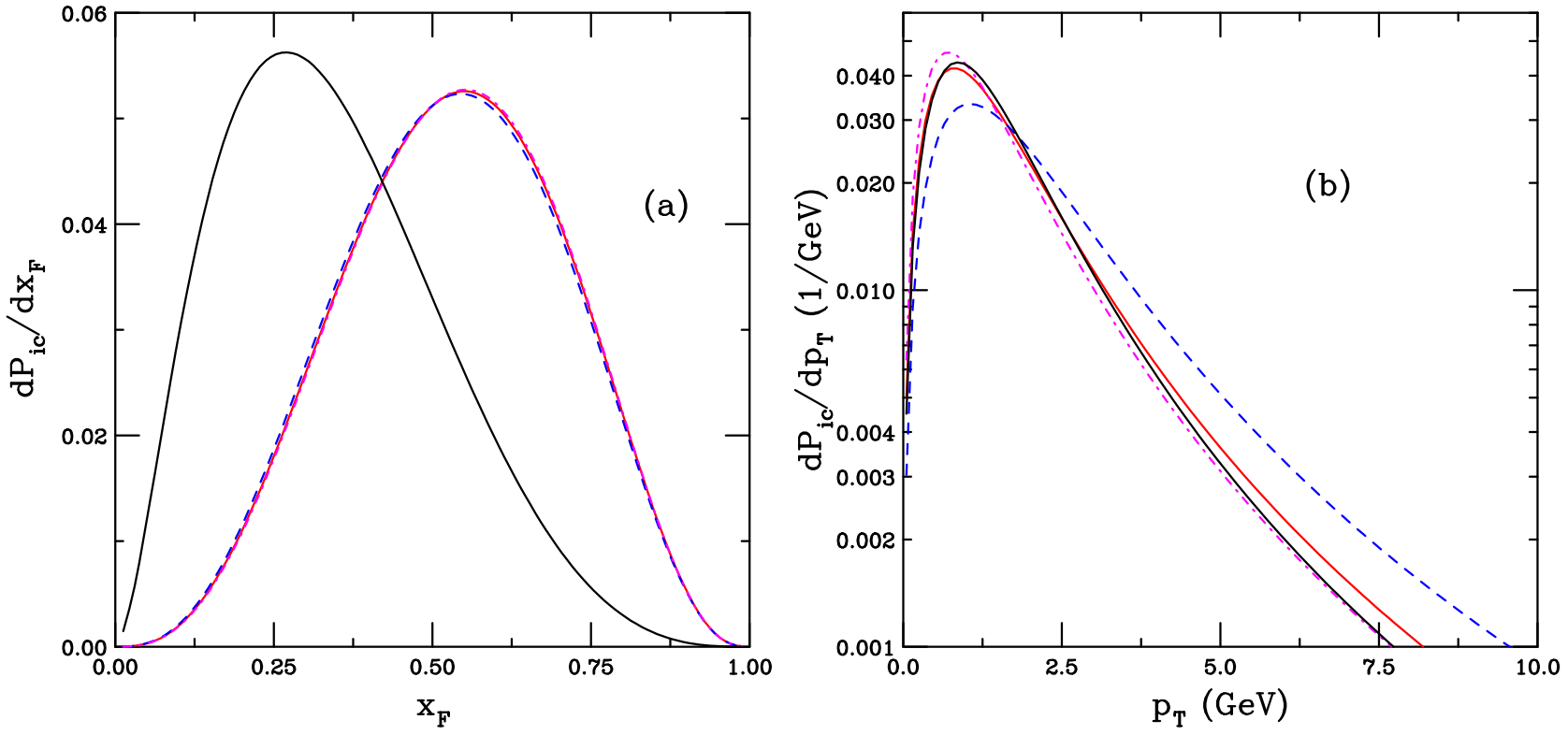

Figure 11: The probability distributions for J/ψ production from a five-particle proton Fock state as a function of x_F (a) and p_T (b). The results are shown for different values of the k_T range for the light and charm quarks. The red curve employs the default values, $k_q^{\max} = 0.2$ GeV and $k_c^{\max} = 1.0$ GeV while the blue dashed curve increases $k_q^{\max}$ and $k_c^{\max}$ by a factor of two and the dot-dashed magenta curve employs half the values of $k_q^{\max}$ and $k_c^{\max}$. The solid black curve shows the x and p_T distributions for a single charm quark from the state.

Intrinsic Charm y Distribution Depends on $\sqrt{s_{NN}}$

Once the x_F distribution is transformed to rapidity, it becomes sensitive to $\sqrt{s_{NN}}$ since $x_F = (2m_T/\sqrt{s_{NN}})\sinh y$

As $\sqrt{s_{NN}}$ increases, the intrinsic charm rapidity distribution is moved further away from midrapidity, taken to the extreme in the right-hand plot, showing the distribution also for $\sqrt{s_{NN}} = 7$ TeV, inaccessible to even most forward detectors

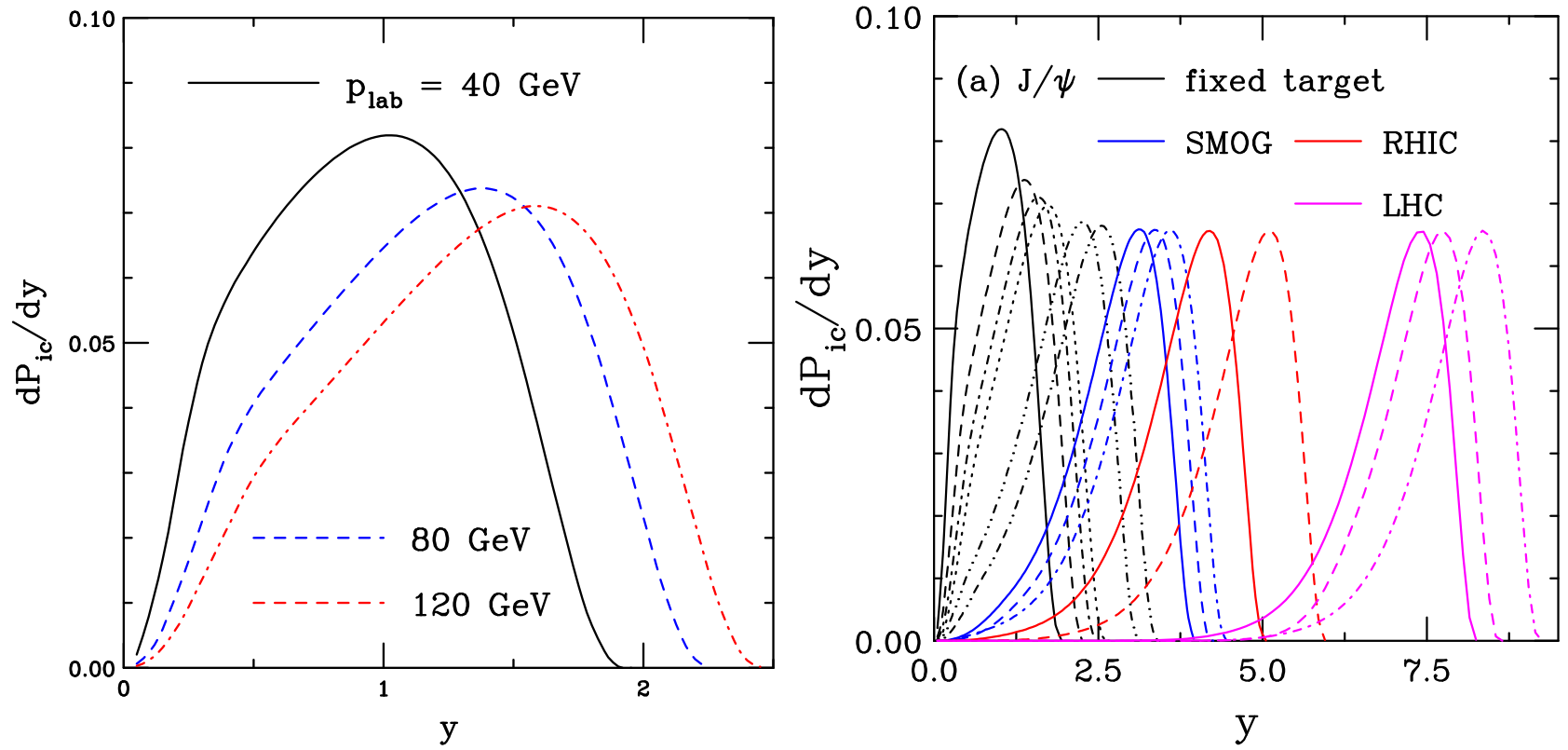

Figure 12: The probability distributions for J/ψ production from a five-particle proton Fock state as a function of y. The results are shown for different values of $\sqrt{s_{NN}}$. The solid black curve shows $\sqrt{s_{NN}} = 8.8$ GeV, the blue dashed curve is for $\sqrt{s_{NN}} = 12.3$ GeV, and the red dot-dashed curve is for $\sqrt{s_{NN}} = 15.4$ GeV. The results in (b) also include the green dotted curve for $\sqrt{s_{NN}} = 7$ TeV.

Observables for Centrality Dependent nPDFs and Intrinsic Heavy Flavors

1. **Impact parameter dependence of nPDFs – is the nucleus made up of shadowing hot spots or is shadowing uniform throughout the nucleus? PHENIX d+Au data suggested the former while ALICE data may suggest the latter. The EIC should study $e + A$ DIS as a function of impact parameter/event multiplicity.**
2. **Intrinsic heavy flavors – $e + p$ EIC measurements could be decisive**

Do Hot Matter Effects Play a Role in $p + A$?

.

Bottomonium Suppression by CNM at the LHC

nPDF effects and energy loss are not final-state dependent: no distinction between ground state and excited states

Absorption and comovers can depend on the final state but at the LHC, absorption will not play a significant role, even at (measurable) backward rapidity because the states are produced well outside the target

Comovers may have more impact on excited states but this is smaller for Υ than for J/ψ

Comovers could be either hadrons or partons (Ferreiro)

The effect in $p+A$ would be larger in the backward region where there are more produced particles

The figure below shows nPDF and energy loss effects only

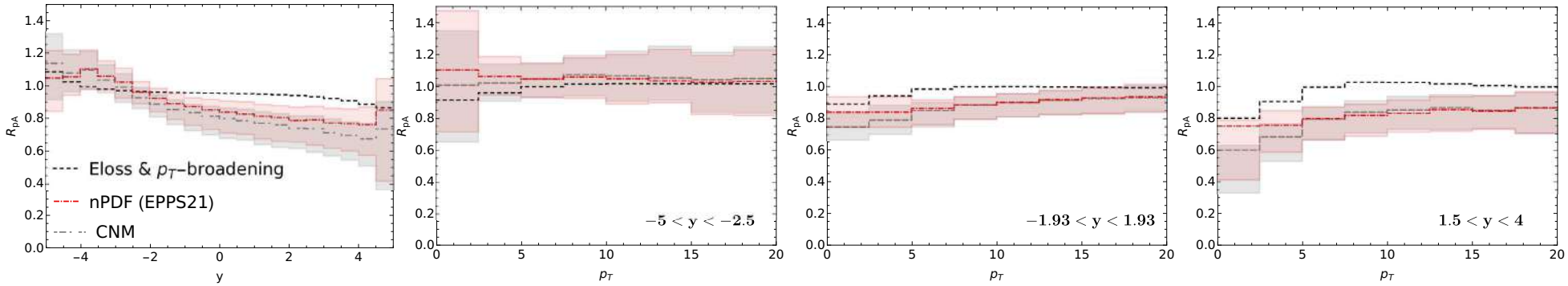

Hot Matter: Open Quantum Systems

NLO pNRQCD open quantum systems approach (PRD 109 (2024) 096016, arXiv:2401.16704 [nucl-th]), labeled KSU-QTraj in figures

- **Quarkonium evolution based on Lindblad equation with dynamics governed by transport coefficients; dissipative and decohering effects encoded in jump operators describing singlet-singlet, singlet-octet and octet-octet transitions, implemented in QTraj code**
- **Differences in suppression for Υ states arises dynamically from state-dependent quantities such as $\langle r^2 \rangle$ and singlet-octet overlaps as well as dependence of the Hamiltonian and width operators on binding energies and level structure**
- **A common medium initialization time $\tau = 0.6$ fm is used for all states**

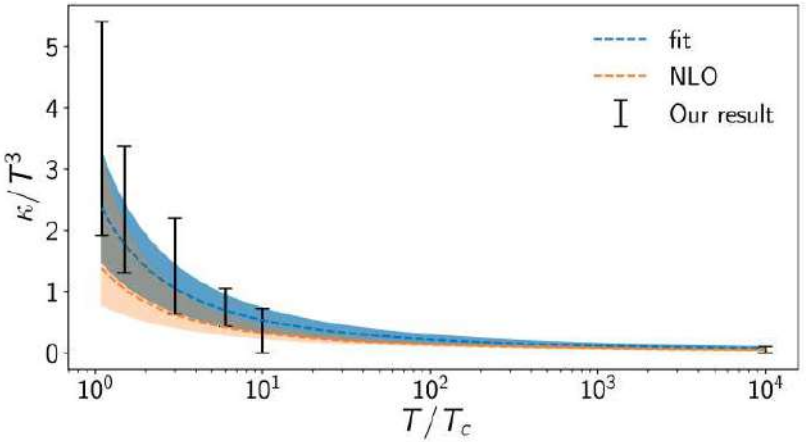

FIG. 13. Temperature dependence of our results compared to the NLO result. The shaded bands include the errors coming from varying the scale by a factor of 2. The blue band also includes the statistical error.

Hot Matter: Semiclassical TAMU Treatments

Rates obtained using two different semiclassical kinetic approaches from the Texas A&M group

- **Quasi-free inelastic scattering and gluo-dissociation employing a perturbative coupling to the medium, labeled TAMU-P in figures**
- **In-medium T-matrix calculations with input potential constrained by lattice QCD calculations of Wilson line correlators, labeled TAMU-NP in figures**
- **Differences in rates and formation times lead to different suppression patterns for Υ states**
- **Regeneration is also considered for TAMU-NP**

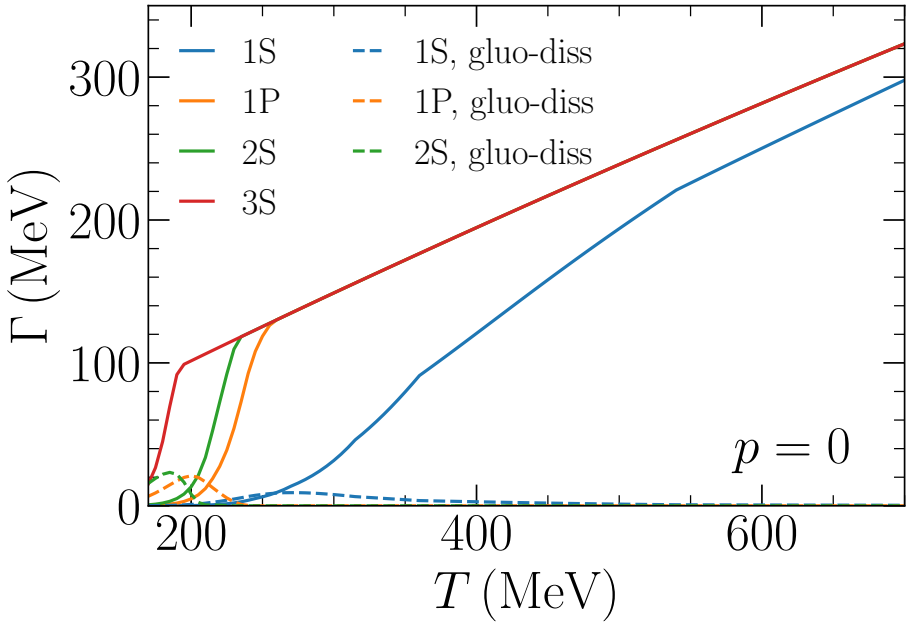

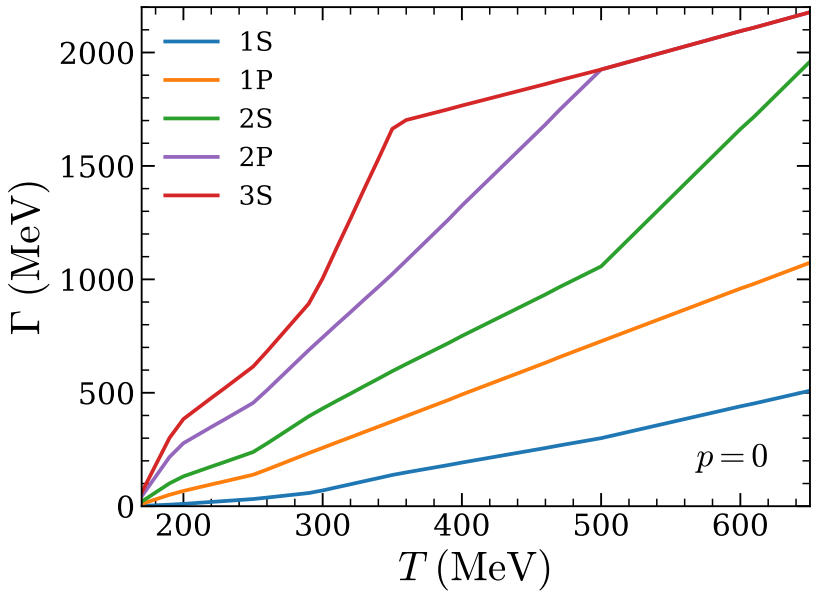

Background Hydrodynamics

Anisotropic nonequilibrium hydrodynamic background calculated using the aHydro3p1 code (arXiv:1807.04337), bottomonium states start interacting with matter after 0.6 fm for open quantum systems (QTraj approach) and after formation time, $\propto 1/E_B$ in TAMU approaches

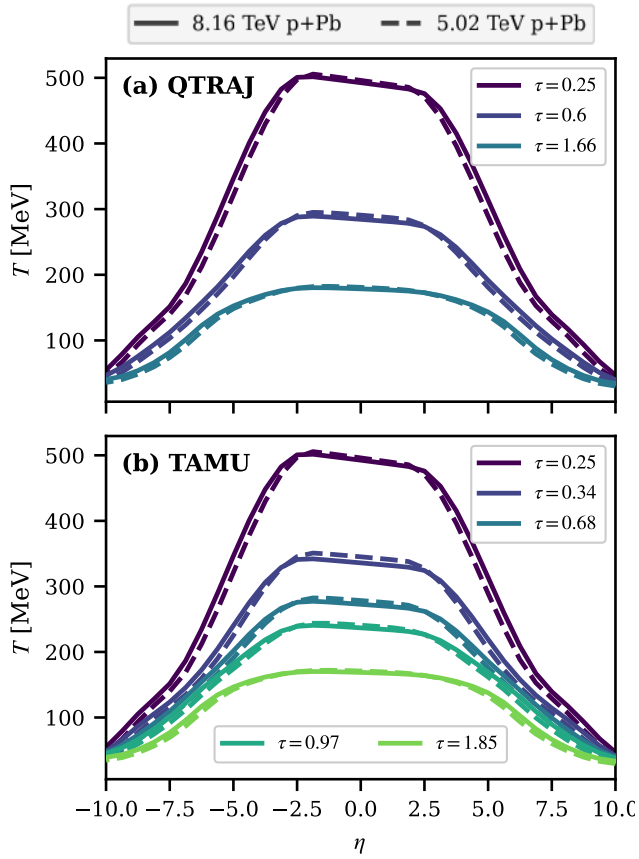

Hot Matter Effects Alone

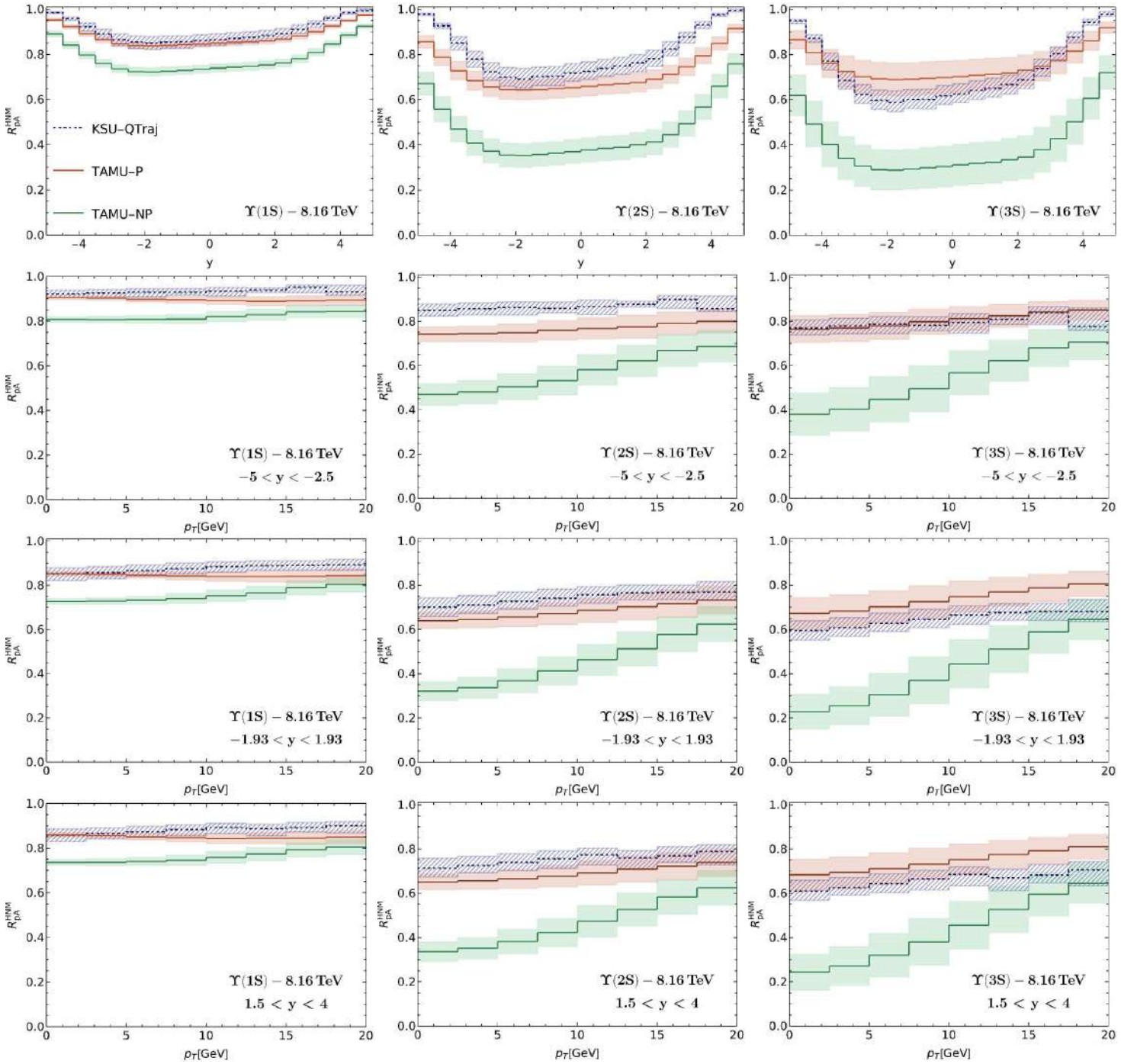

Combined Suppression, without and with Regeneration

Rapidity dependence with both CNM and hot matter effects shown

TAMU-NP rates significantly increase suppression, adding regeneration helps bring the results closer to data

Smaller TAMU-P rates would also reduce regeneration; QTraj results include regeneration when transitions are taken into account

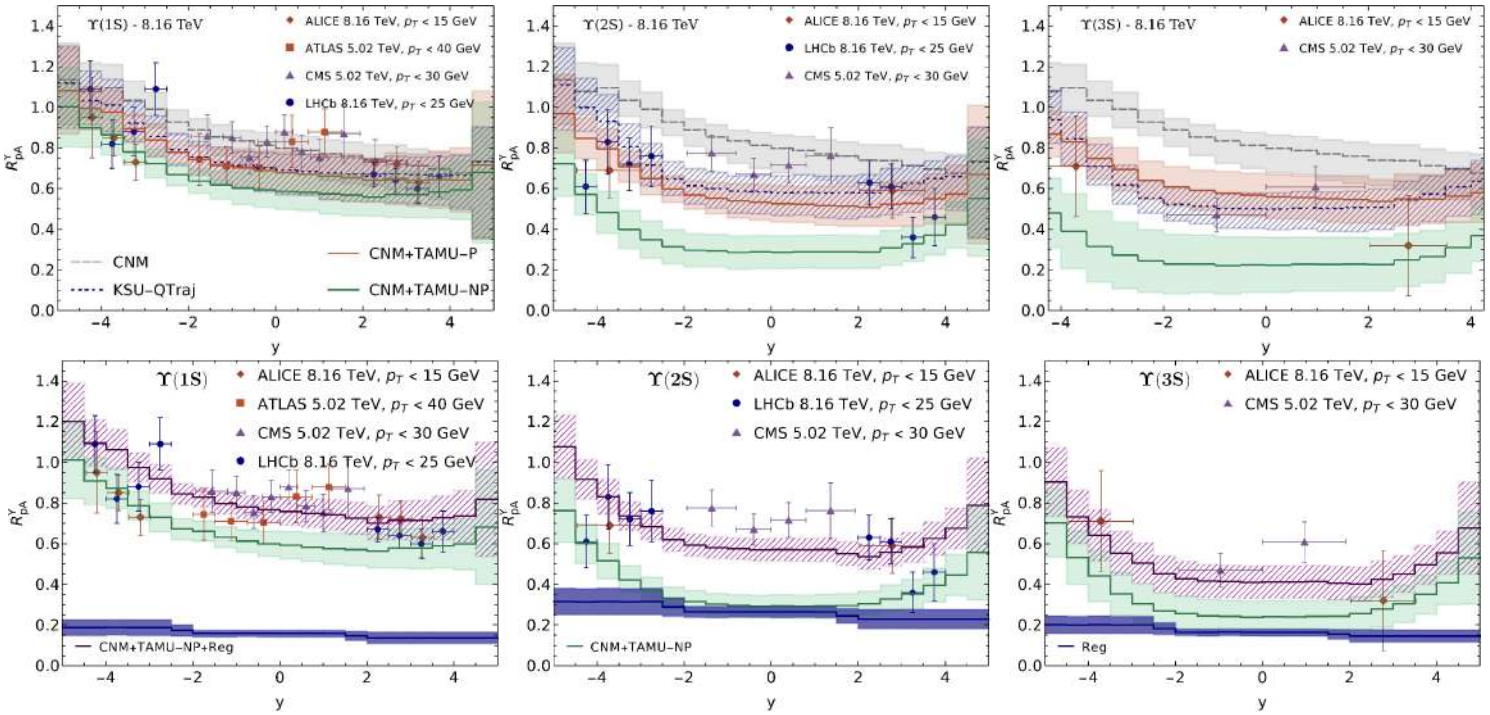

Extending Calculations to Charmonium

Calculations will treat both the LHC and RHIC

Only cold matter effects are included so far, the calculation is still in progress.

Impact parameter dependent shadowing is included; uncertainties introduced for energy loss and k_T broadening

Same hydro background is used but centrality dependence needs to adopted

Absorption will be included for RHIC energies

Only TAMU rates will be used here: no open quantum systems calculation exists for charmonium

Centrality Dependent CNM Effects vs y

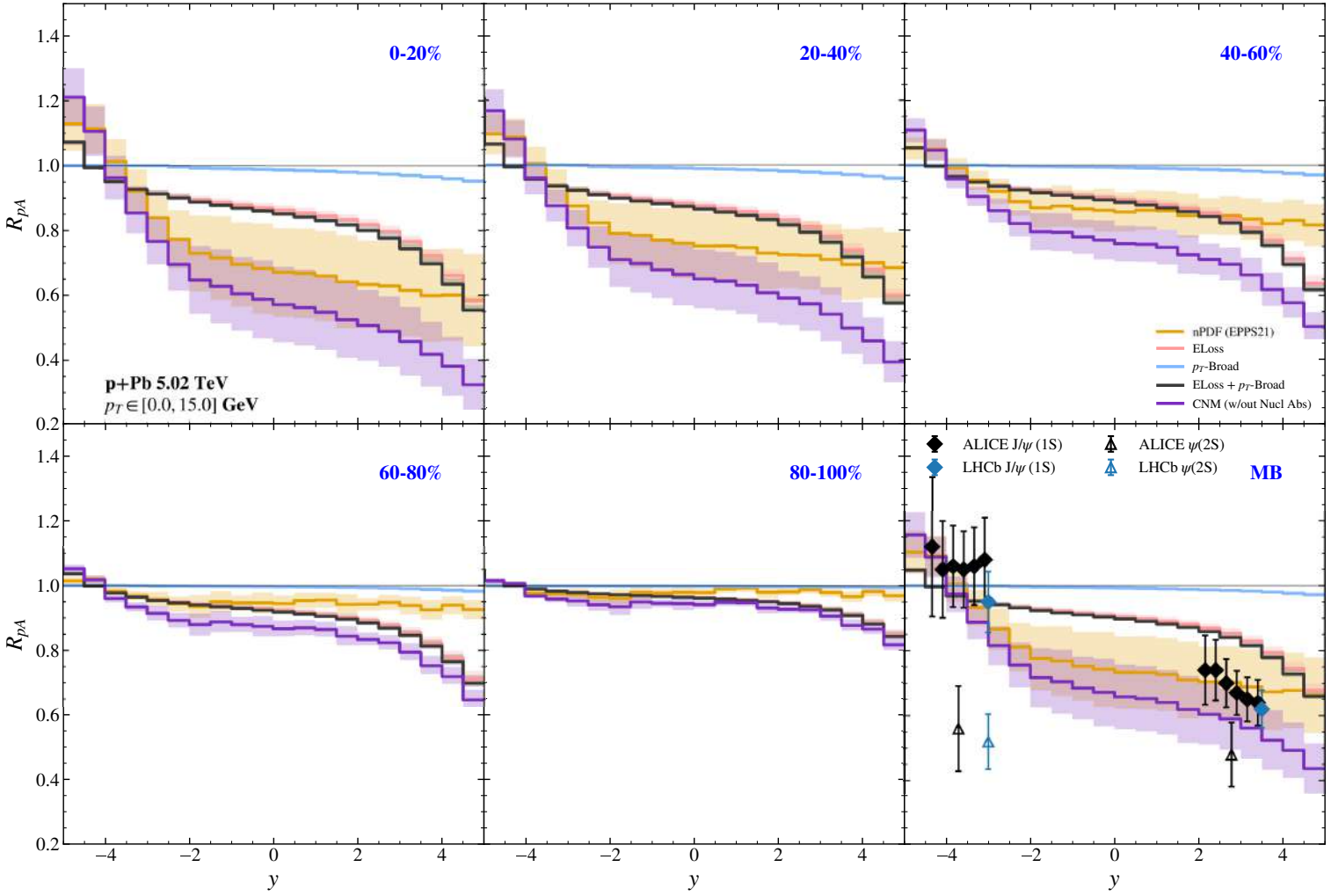

Centrality Dependent CNM Effects vs p_T in 3 y Bins

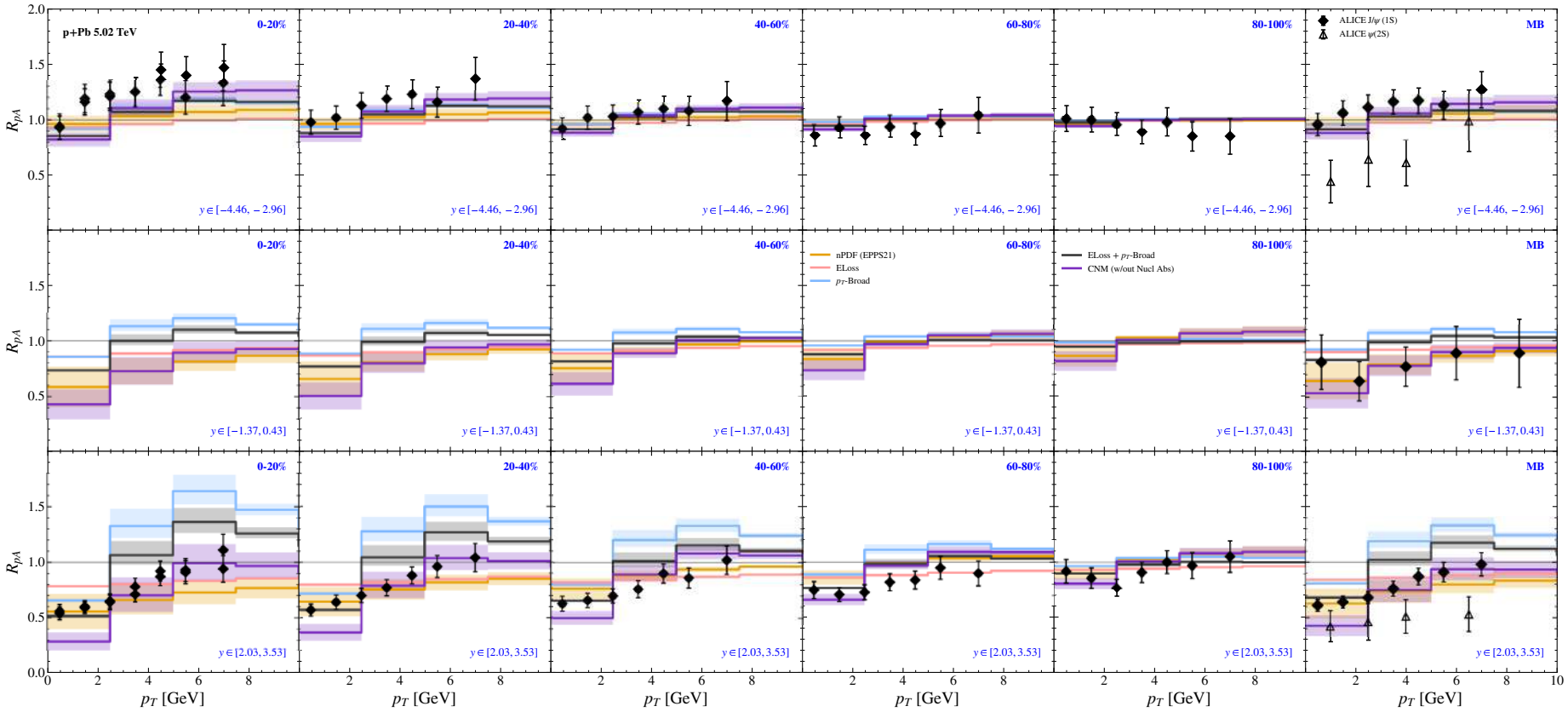

Using the EIC to Further Disentangle Cold and Hot Matter Effects

.

A Fixed-Target Program at the EIC

Conceptual notion of the EIC collision region with a fixed target

In the A-going direction (left) particle from fixed target $p + A$ and $A + A'$ collisions can be measured, top energy of $\sqrt{s_{NN}} \sim 14$ GeV for 100 GeV/nucleon Au beam

Cross sections for space radiation protection can also be measured

Either a gas jet target (like SMOG@LHCb) or target wires (like STAR BES II) can be used; likely target wires in ePIC

See the white paper, arXiv:2603.00265, and workshop website https://indico.cfnssbu.physics.sunysb.edu/event/496/

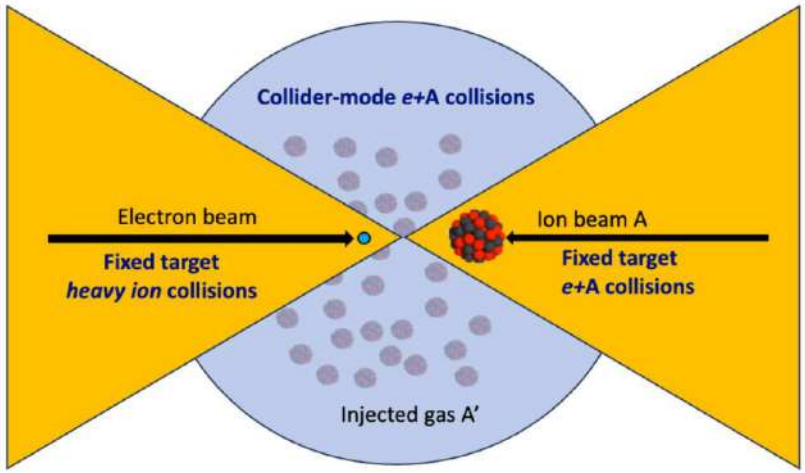

Putting the Possible Energy Range Into Perspective: $p + A$

The maximum energy of the proton beam is 250 GeV; minimum is in principle the injection energy, giving a range of potential $p + A$ energies, $\sqrt{s_{NN}} \sim 7 - 21.7$ GeV.

This range is bigger than that planned for NA60+ at the SPS and covers the lower range of NA50 to well below the energy of E906 (SeaQuest, $p_{\mathrm{beam}} = 120$ GeV)

In addition to cold matter studies, these measurements would provide the missing baseline from at least some of the STAR Beam Energy Scan II measurements

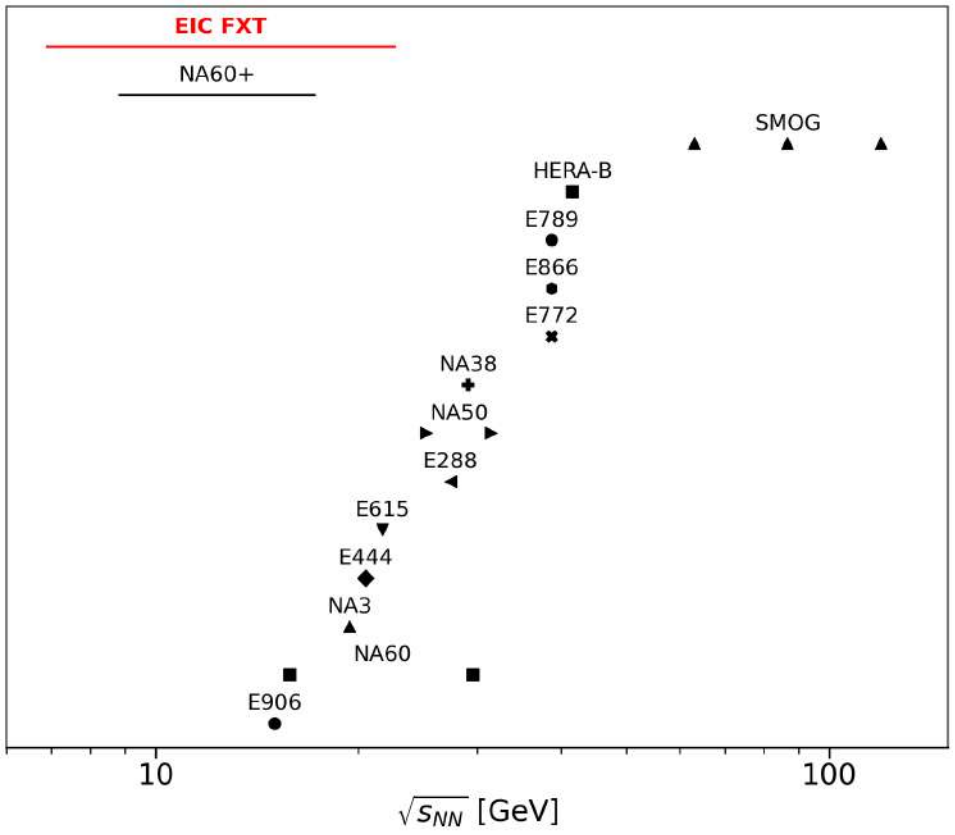

Putting the Possible Energy Range Into Perspective: $A + A'$

The maximum energy of a gold beam is 100 GeV; minimum is in principle the injection energy, giving a range of potential $p + A$ energies, $\sqrt{s_{NN}} \sim 3 - 14$ GeV.

This range covers the same area as the STAR Fixed-Target program in the Beam Energy Scan II studies but provides the opportunity to extend it to higher energies and nuclear targets other than gold

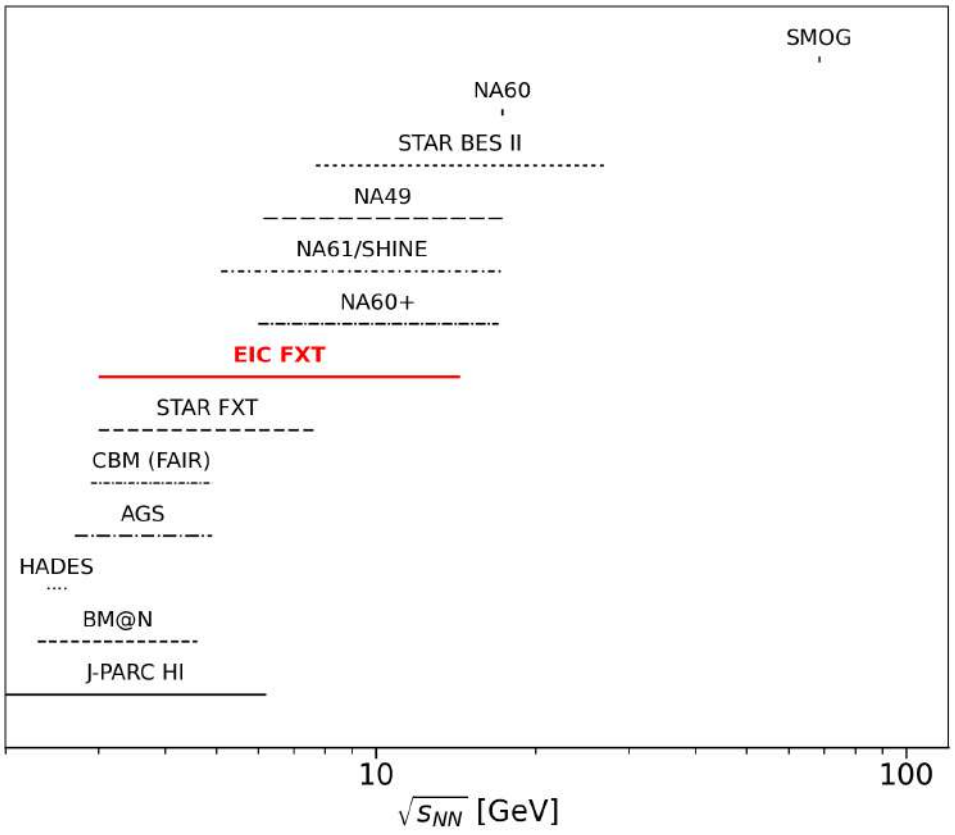

Target Wires vs. Gas Jet Target?

Target Wires (STAR BES II runs)

- **Wires have to be installed and left in place**
- **Target wheel could add multiple potential targets**
- **Can't be run parasitically, separate runs required to steer beam onto the targets**

Gas Jet (LHCb SMOG setup)

- **The SMOG device uses noble or neutral gases (^{4}He, Ne, Ar (Kr, Xe possible) and H_2, O_2, and N_2)**
- **Gases can be continuously injected and changed easily**
- **Can be run parasitically, LHCb has collected large datasets with the new SMOG2 setup**

Advantages to both but ideally more than one single target would be used: a lever arm in A is useful, both for understanding cold matter effects and for space radiation studies (C, Si, Al preferred relative to Au)

Putting Target Wires in ePIC

Placing the target in the backward region ($z = -3290$ mm relative to the interaction point) exploits the forward detector systems

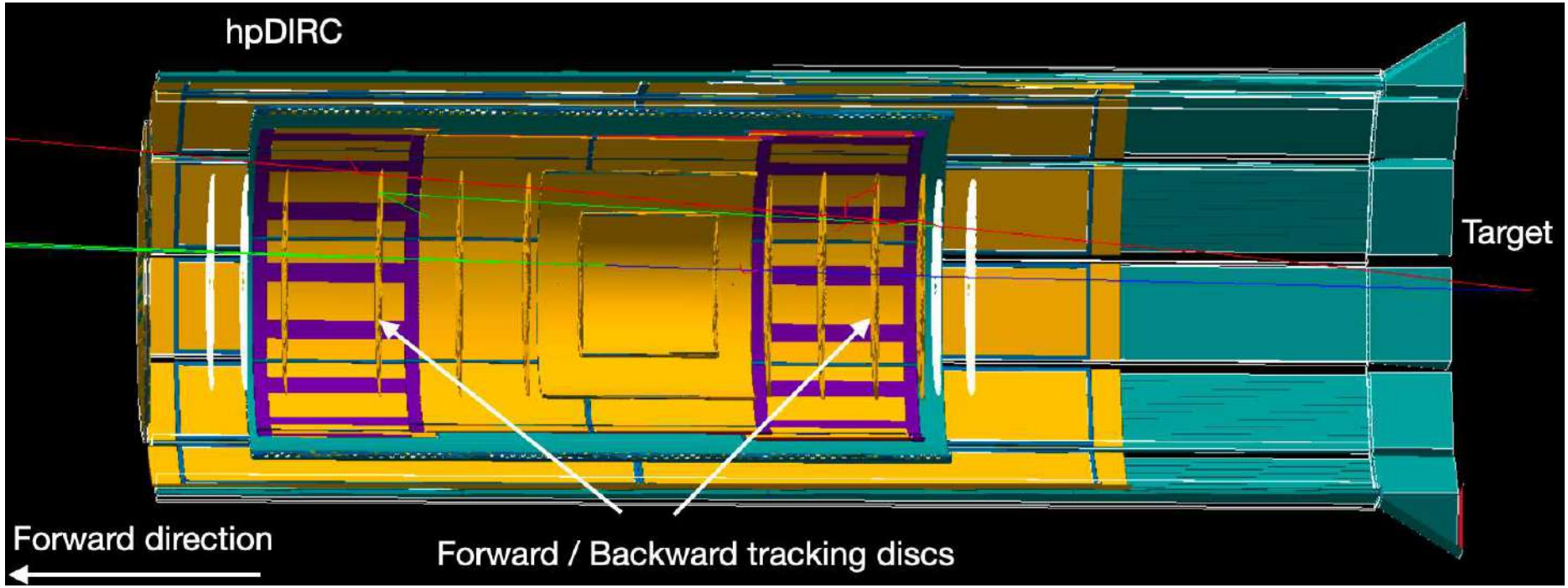

Some Idealized Example Simulations

Simulations in arXiv:2603.00265 assumed $p + p$ collisions for simplicity

A 200 GeV proton beam was assumed for $\sqrt{s} = 19.4$ GeV

Studied charged pion and J/ψ acceptance, with pion and muon (from J/ψ decays) tracks with at least 4 hits in the tracker

Pion acceptance in η and p_T studied for two different target positions

J/ψ acceptance in m_T and x_2 studied for single target position

ePIC Phase Space Coverage Depends on Target Location

Placing the target in the backward region ($z = -3290$ mm relative to the interaction point) exploits the forward detector systems

With target in the backward region, left, acceptance is forward of midrapidity, reaches lower x_2 (and higher p_T) but may be less useful as baseline for STAR BES II

Putting the target at $z = 0$ (at the reaction point), right, would allow measurements closer to midrapidity but generally at lower p_T

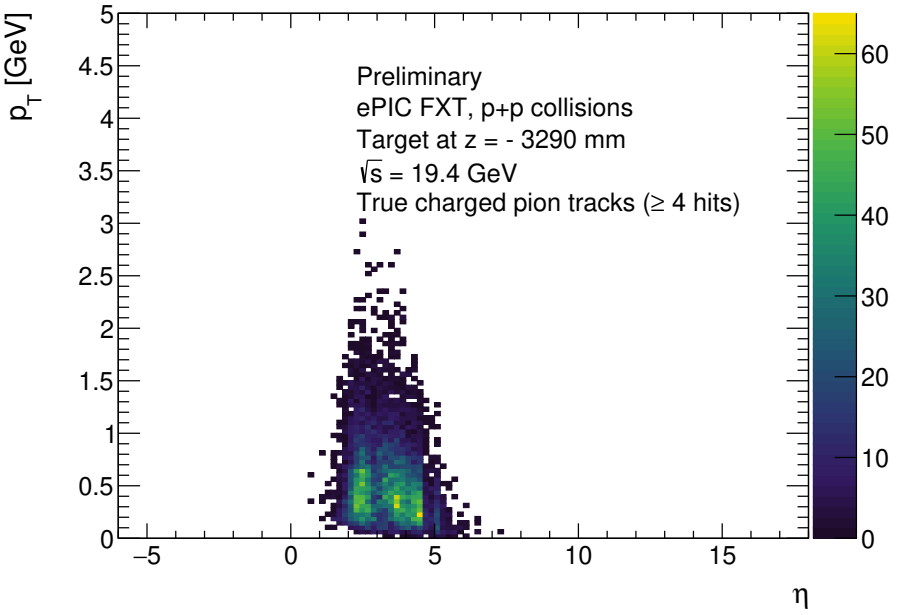

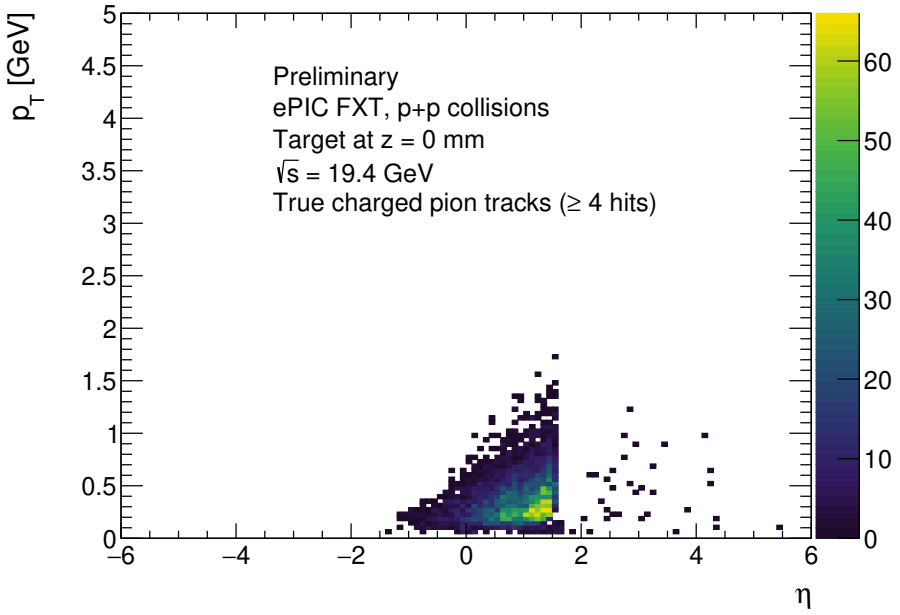

J/ψ x_2 Coverage

In the configuration where the target is backward of the interaction point, $0.02 < x_2 < 0.4$**, in the antishadowing region,** $m_T \sim 4.5$ **GeV implies** $p_T \sim 3.5$ **GeV**

With the target at the interaction point, x_2 **would be larger**

Going to lower energies would move acceptance to higher x_2**, lower** m_T**, as well as changing the balance of production from** gg **dominated (still) at the higher energy to** $q\overline{q}$ **dominance at the low energy end of** $\sqrt{s_{NN}}$ **range**

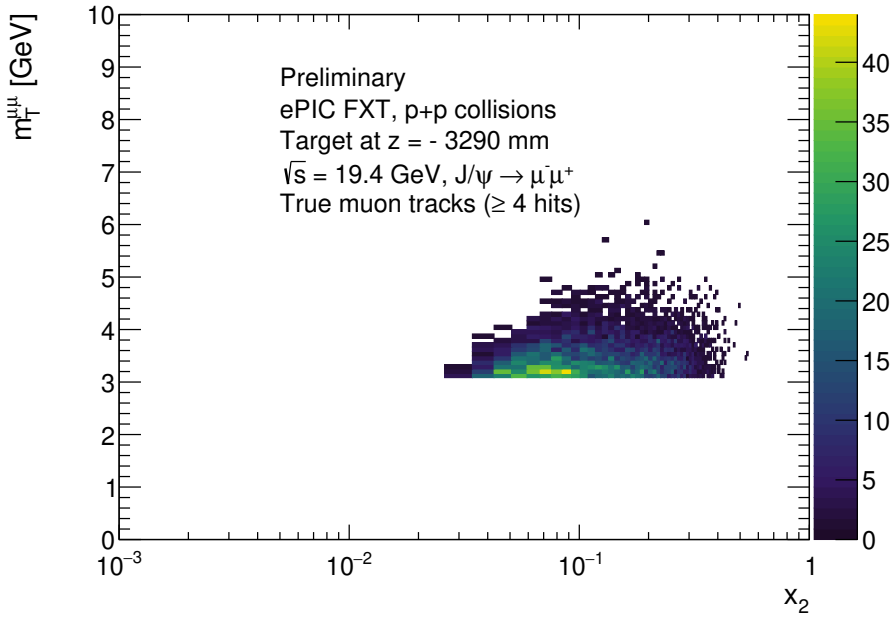

A Definitive Measurement of Intrinsic Charm at the EIC?

.

IC Potentially Easier to Measure in Fixed-Target Experiments

As $\sqrt{s_{NN}}$ increases, the intrinsic charm rapidity distribution is moved further away from midrapidity, at collider energies it is inaccessible to most forward detectors

The p_T distributions are shown with the rapidity range is restricted to $0 < y < 1$, green curve shows integration over all y; if y acceptance at higher y, more of the IC p_T distribution is captured

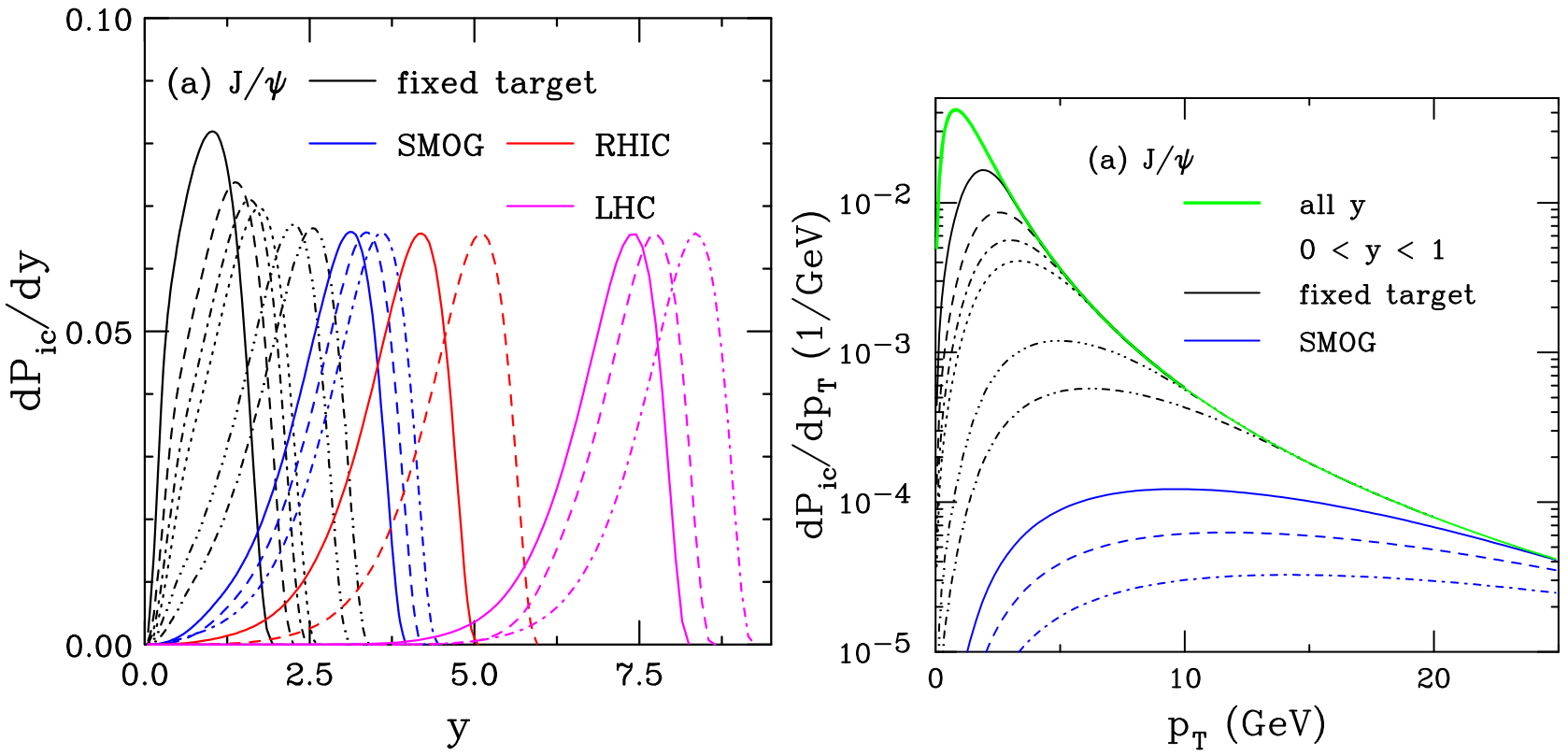

Figure 13: The probability distributions for J/ψ production from a five-particle proton Fock state as a function of y (left) and p_T (right). The rapidity distributions are shown for $\sqrt{s} = 8.8$ GeV to 13 TeV. (Right) The results are shown for all rapidity in the solid green curve. Results for restricting the rapidity range to $0 < y < 1$ are shown for $p_{\rm lab} = 40$, 80 and 120 GeV by the solid black, dashed blue and dot-dashed red respectively.

Recent and Forthcoming Fixed-Target Experiments Ideal for IC Studies

Many previous experiments studied J/ψ production off nuclear targets at proton beam energies from 158 to 920 GeV, several used to get a baseline for $A + A$ collisions; those that covered large x_F saw a larger suppression of production off nuclear targets at higher x_F

SeaQuest: Took data with a 120 GeV proton beam on p, d, C, Fe, and W targets, covered forward region, $0.4 < x_F < 0.95$ and $p_T < 2.3$ GeV; J/ψ data not published yet but should report nuclear suppression factor, $pA/p\mathrm{d}$

SMOG: Gas jet target in LHCb, J/ψ and D^0 measured at backward rapidity in the fixed-target center of mass, data so far at: $p + \mathrm{Ne}$ at $\sqrt{s_{NN}} = 68.5$ GeV; $p + \mathrm{He}$ at $\sqrt{s_{NN}} = 86.6$ GeV; and $p + \mathrm{Ar}$ at $\sqrt{s_{NN}} = 110.4$ GeV

NA60+: proton beams at $p_{\mathrm{lab}} = 40$, 80, and 120 GeV, nuclear targets from Be to Pb

EIC: proton beams up to 250 GeV, gold beams up to 100 GeV; targets to be defined

Calculations and comparison to data in the following from R. Vogt, arXiv:2101.02858, Phys. Rev. C 103, 035204 (2021); arXiv:2207.04347, Phys. Rev. C 106, 025201 (2022); arXiv:2304.03451, Phys. Rev. C 108, 015201 (2023)

Summary of Previous Fixed-Target J/ψ Data

NA60 $p_{\rm lab} = 158$ **and 400 GeV, covering** $0.05 < x_F < 0.4$ **and** $-0.075 < x_F < 0.125$ **respectively, were taken on Be, Al, Cu, In, W, Pb, and U targets (PLB 706, 263 (2012))**

NA3 $p_{\rm lab} = 200$ **GeV,** $x_F > 0$**, taken on a Pt target (Z. Phys. C 20, 101 (1983))**

NA50 $p_{\rm lab} = 450$ **GeV, midrapidity** $(-0.1 < x_F < 0.1)$**, used Be, Al, Cu, Ag, W and Pb targets (EPJ C 33, 31 (2004))**

E866 $p_{\rm lab} = 800$ **GeV,** $-0.09 < x_F < 0.95$**, used Be, Fe, and W targets (PRL 84, 3256 (2000))**

HERA-B $p_{\rm lab} = 920$ **GeV,** $-0.34 < x_F < 0.14$**, used C, Ti and W targets (EPJ C 60, 525 (2009))**

E866 J/ψ x_F and p_T Distributions $(p+p)$

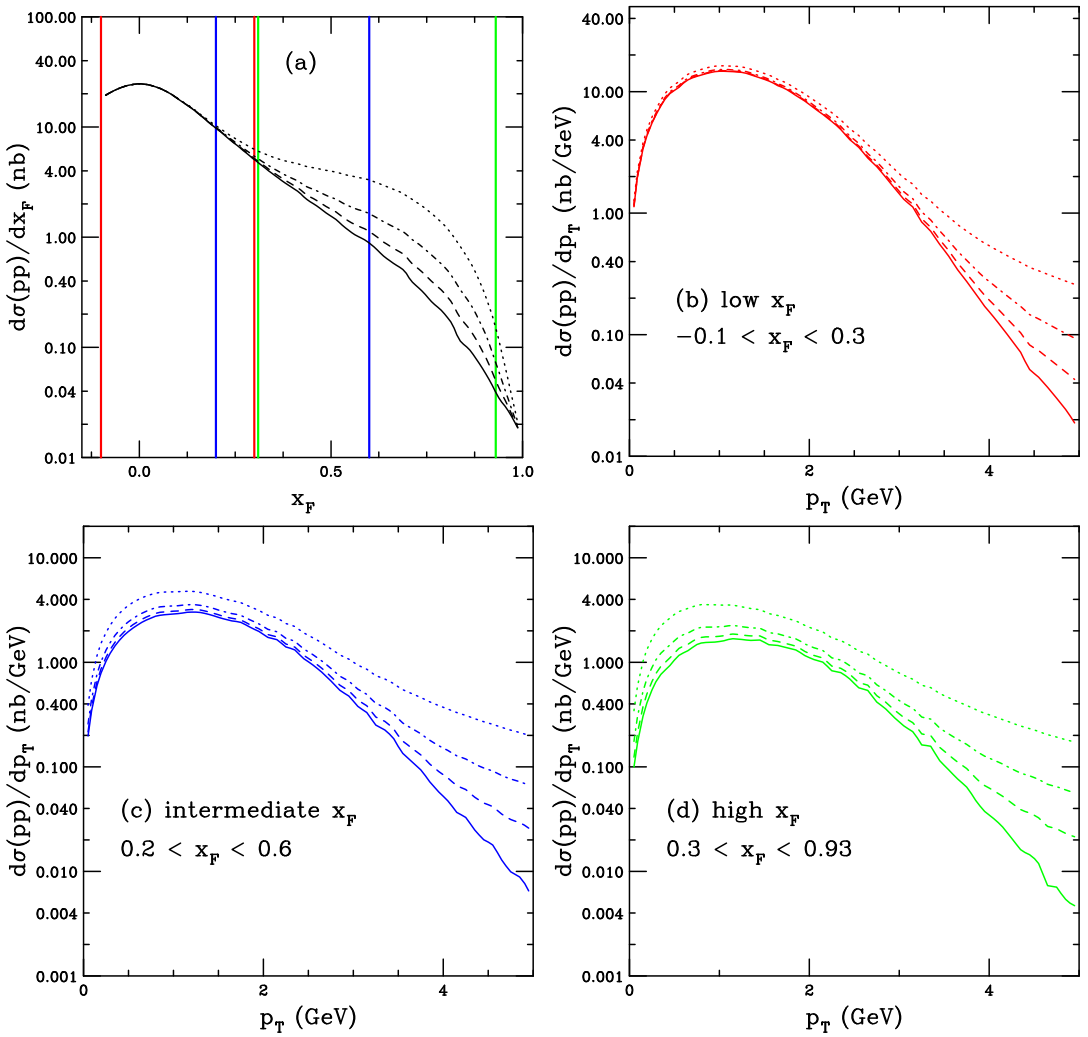

Figure 14: The J/ψ cross sections in $p+p$ collisions at $\sqrt{s} = 38.8$ GeV with and without IC as a function of x_F (a) and p_T at low (b), intermediate (c), and high x_F (d). The solid curves do not include IC while the dashed, dot-dashed and dotted curves use $P^0_{\mathrm{ic}\,5} = 0.1\%$, 0.31% and 1% respectively. The colored vertical bars on the x_F distributions show the x_F limits of the p_T distributions in (b)-(d) and matches the color of the curves in (b)-(d). RV, PRC **103**, 035204 (2021).

Comparison with α Extracted from E866 J/ψ $p+A$ Data

E866 obtained α as a function of x_F and p_T (in 3 x_F bins) for $A =$ Be, Fe, and W

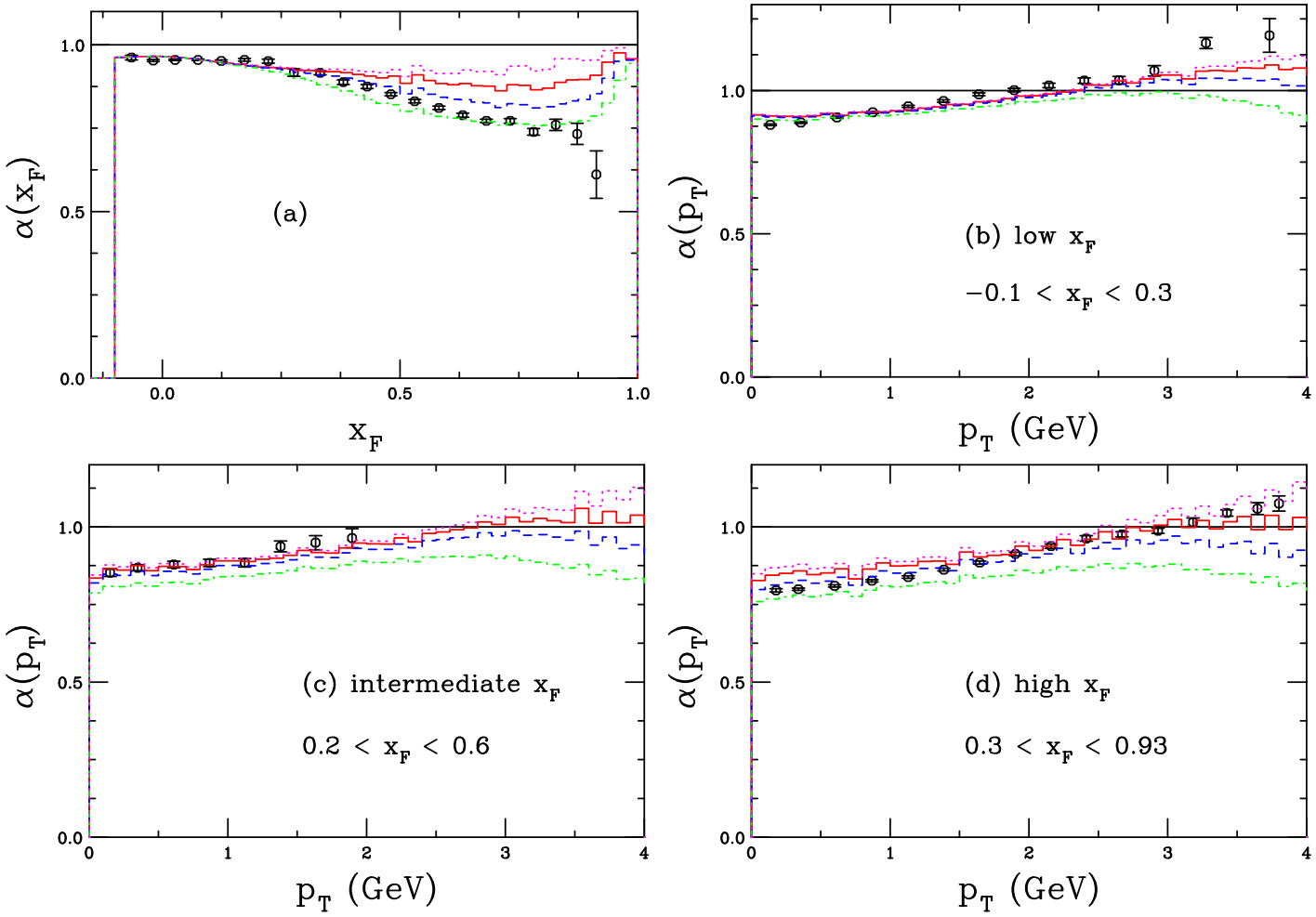

Figure 15: The exponent $\alpha(x_F)$ (a) and $\alpha(p_T)$ for low x_F (b), intermediate x_F (c), and high x_F (d). The dotted magenta curves use $P^0_{\rm ic\,5} = 0$ while the solid red, dashed blue, and dot-dashed green curves show $P^0_{\rm ic\,5} = 0.1\%$, 0.31% and 1% respectively. The E866 data (PRL **84**, 3256 (2000)) are the black points. From: RV, PRC **103**, 035204 (2021).

Comparison of $\alpha(x_F)$ with Fixed-Target J/ψ Data

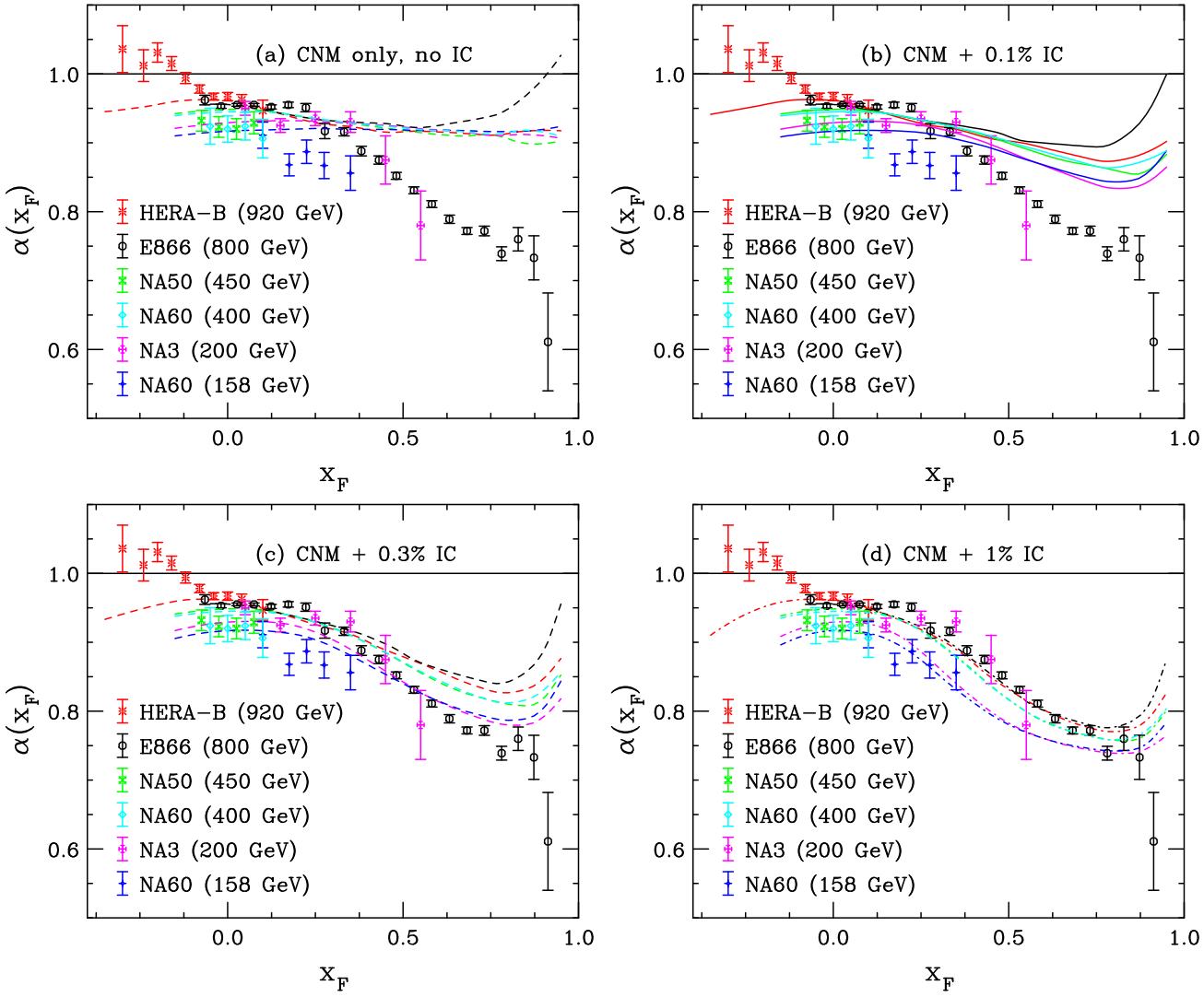

Figure 16: The value of $\alpha(x_F)$ for J/ψ production at: NA60 ($p_{\rm lab} = 158$ GeV), NA3 ($p_{\rm lab} = 200$ GeV), NA60 ($p_{\rm lab} = 400$ GeV), NA50 ($p_{\rm lab} = 450$ GeV), E866 ($p_{\rm lab} = 800$ GeV), and HERA-B ($p_{\rm lab} = 920$ GeV). The points and curves of the same color are at the same energy. Calculations with $P^0_{\rm ic\,5} = 0$ are in (a) while $P^0_{\rm ic\,5} = 0.1\%$, 0.3%, and 1% are shown in (b)-(d).

SMOG J/ψ Results Compared to Calculations

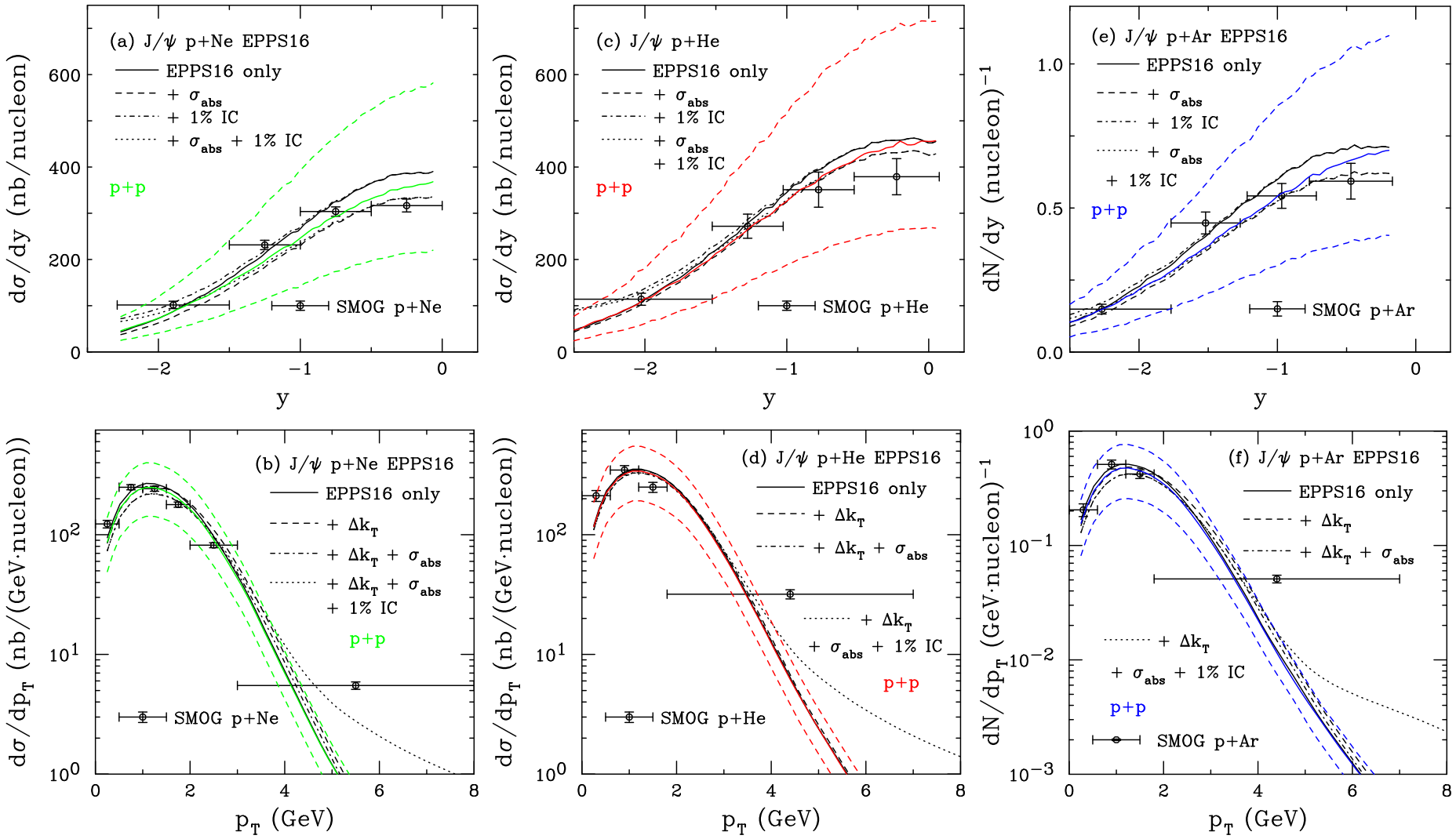

Figure 17: The J/ψ cross section as a function of y in (a), (c), (e) and p_T in (b), (d), (f) for p+Ne ($\sqrt{s_{NN}} = 68.5$ GeV) in (a) and (b); p+He ($\sqrt{s_{NN}} = 86.6$ GeV) in (c) and (d); and $p + $ Ar ($\sqrt{s_{NN}} = 110.4$ GeV) in (e) and (f). The black curves are the $p + A$ calculations. The colored curves (solid and dashed) show the CEM $p + p$ calculations (no IC). The $p + A$ rapidity distributions are shown for EPPS16 only (solid); EPPS16 with absorption (dashed); EPPS16 and $P^0_{\rm ic\,5} = 1\%$ (dot-dashed); and EPPS16, absorption, and $P^0_{\rm ic\,5} = 1\%$ (dotted). The p_T distributions show EPPS16 only (solid); EPPS16 with k_T kick (dashed); EPPS16, absorption, and k_T kick (dot-dashed); and EPPS16, absorption, k_T kick and $P^0_{\rm ic\,5} = 1\%$ (dotted). The $p + $ Ne data are from arXiv:2211.11645; the $p + $ He and $p + $ Ar data are from PRL **122**, 132002 (2019).

$p+p$ distributions as a function of y and p_T: With and Without Intrinsic Charm

All p_T calculations assume integration over all y, the intrinsic charm contribution would be overestimated if the contribution would be restricted to midrapidity – this effect becomes larger at higher energies, there would be no contribution to the midrapidity p_T distribution at all at RHIC and LHC energies

The strong energy dependence of the intrinsic charm contribution is evident; any pQCD nuclear effects would be quickly overwhelmed

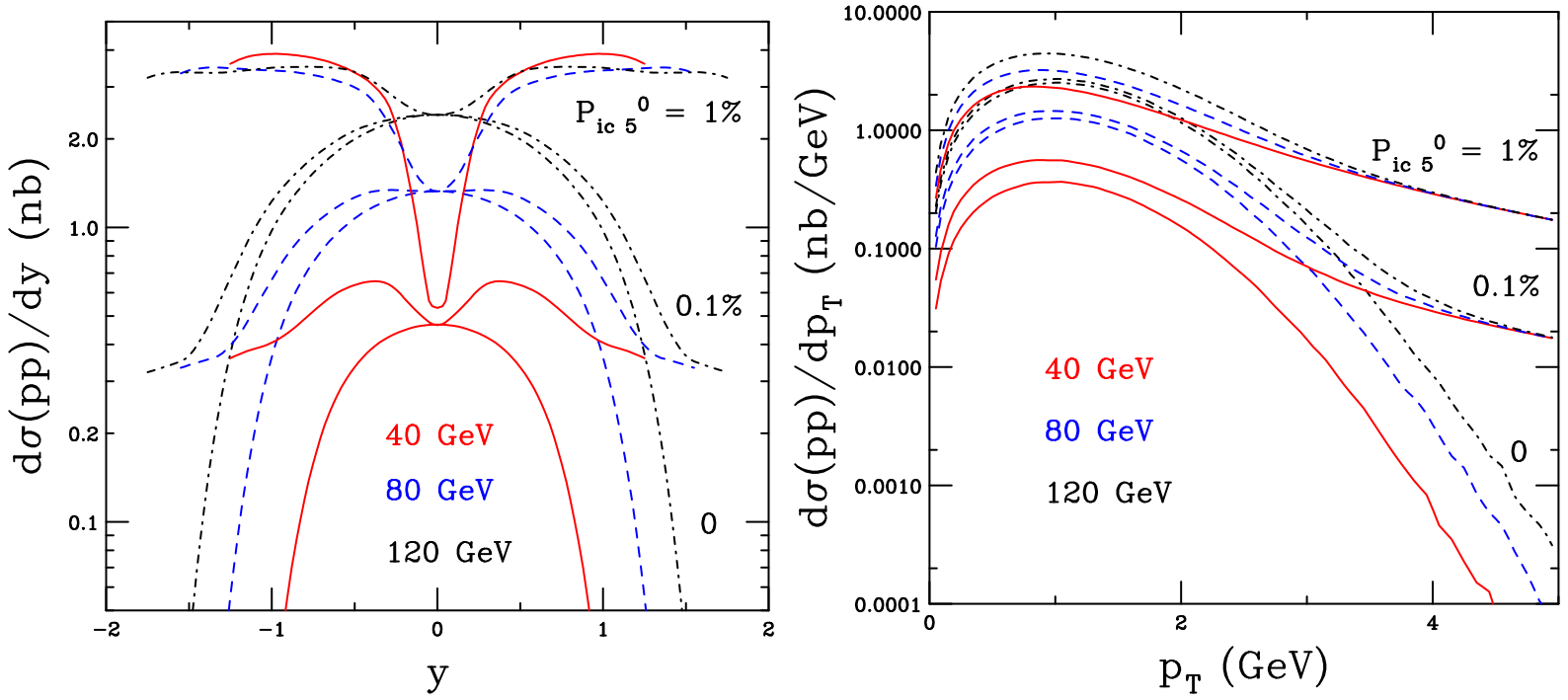

Figure 18: The nuclear modification factors for J/ψ production as a function of y (left) and p_T (right) in $p+p$ collisions with $P^0_{\rm ic\,5} = 0\%$ (bottom curves) 0.1% (middle curves) and 1% (upper curves). The solid red, blue dashed and black dot-dashed curves are for $p_{\rm lab} = 40$, 80 and 120 GeV respectively.

Rapidity and p_T $p + \mathrm{Pb}$ Ratios: No Intrinsic Charm

Upper curves do not include absorption, lower curves employ $\sigma_{\rm abs} = 9$, 10 and 11 mb for $p_{\rm lab} = 120$, 80 and 40 GeV respectively

Rapidity distributions do not depend on k_T kick, only absorption, increasing beam energy broadens rapidity distribution, increasing absorption gives lower $R_{p\rm Pb}$

p_T distributions without k_T kick flat, higher incident energy goes further into anti-shadowing region, increasing energy also increases size of k_T kick

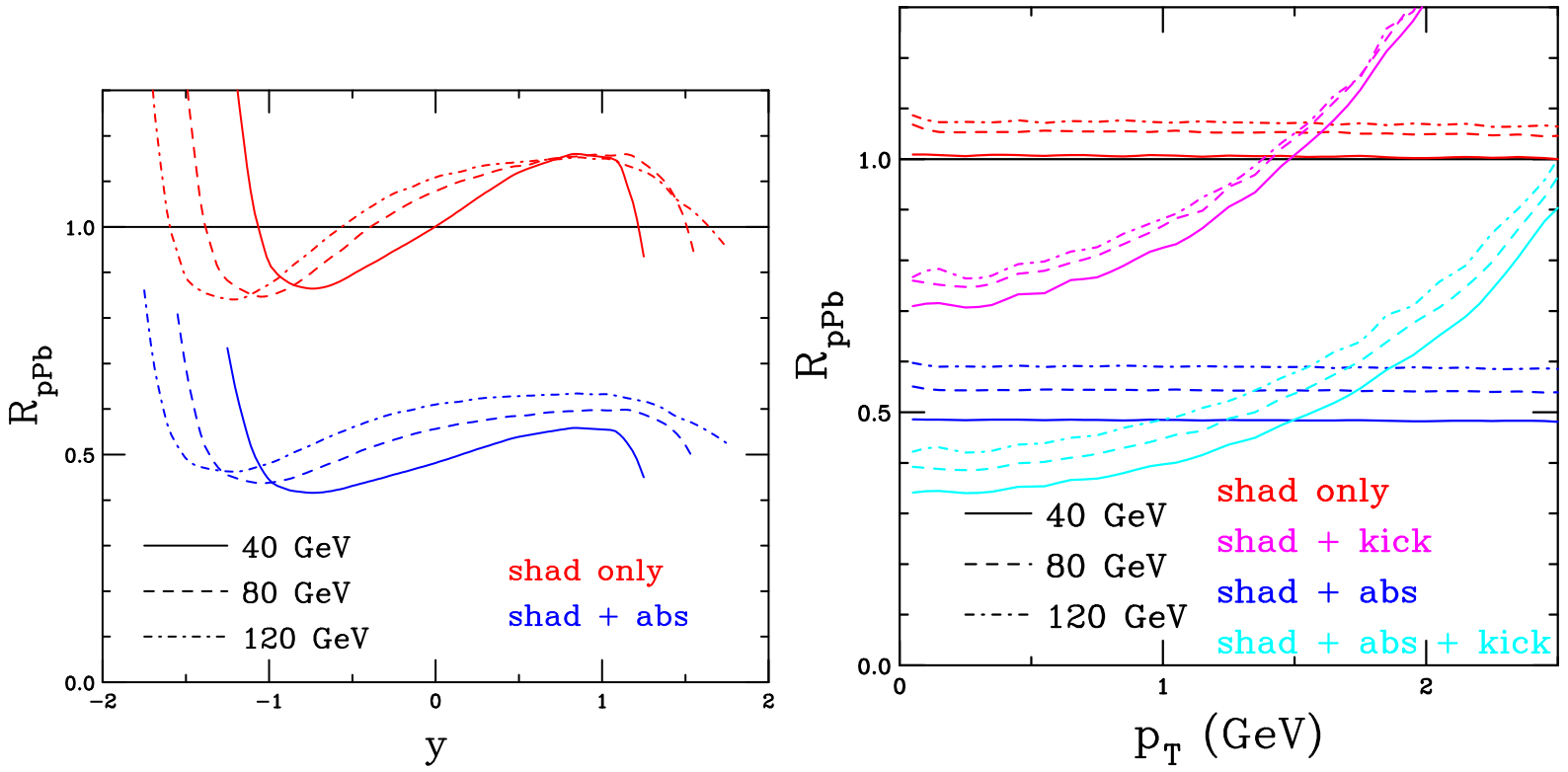

Figure 19: The nuclear modification factors for J/ψ production as a function of y (left) and p_T (right) for pQCD production alone for lead targets relative to proton. The solid, dashed and dot-dashed curves are for $p_{\rm lab} = 40$, 80 and 120 GeV respectively. The curves are for nPDF effects alone (red), nPDFs with an additional k_T kick (magenta), nPDFs and absorption (blue), and nPDFs, absorption and k_T broadening (cyan). Note that the rapidity distributions do not depend on the k_T broadening.

$R_{p\mathrm{Pb}}$ as a function of y: With Intrinsic Charm

Upper curves do not include absorption, lower curves employ $\sigma_{\mathrm{abs}} = 9$, 10 and 11 mb for $p_{\mathrm{lab}} = 120$, 80 and 40 GeV respectively

At these energies, $R_{p\mathrm{Pb}}$ is overwhelmed by intrinsic charm, even at midrapidity with $P^0_{\mathrm{ic}\,5} = 0.1\%$, unlike higher energy E866 results

At low center of mass energies, the rapidity distribution is not boosted very much. The energy dependence is quite strong.

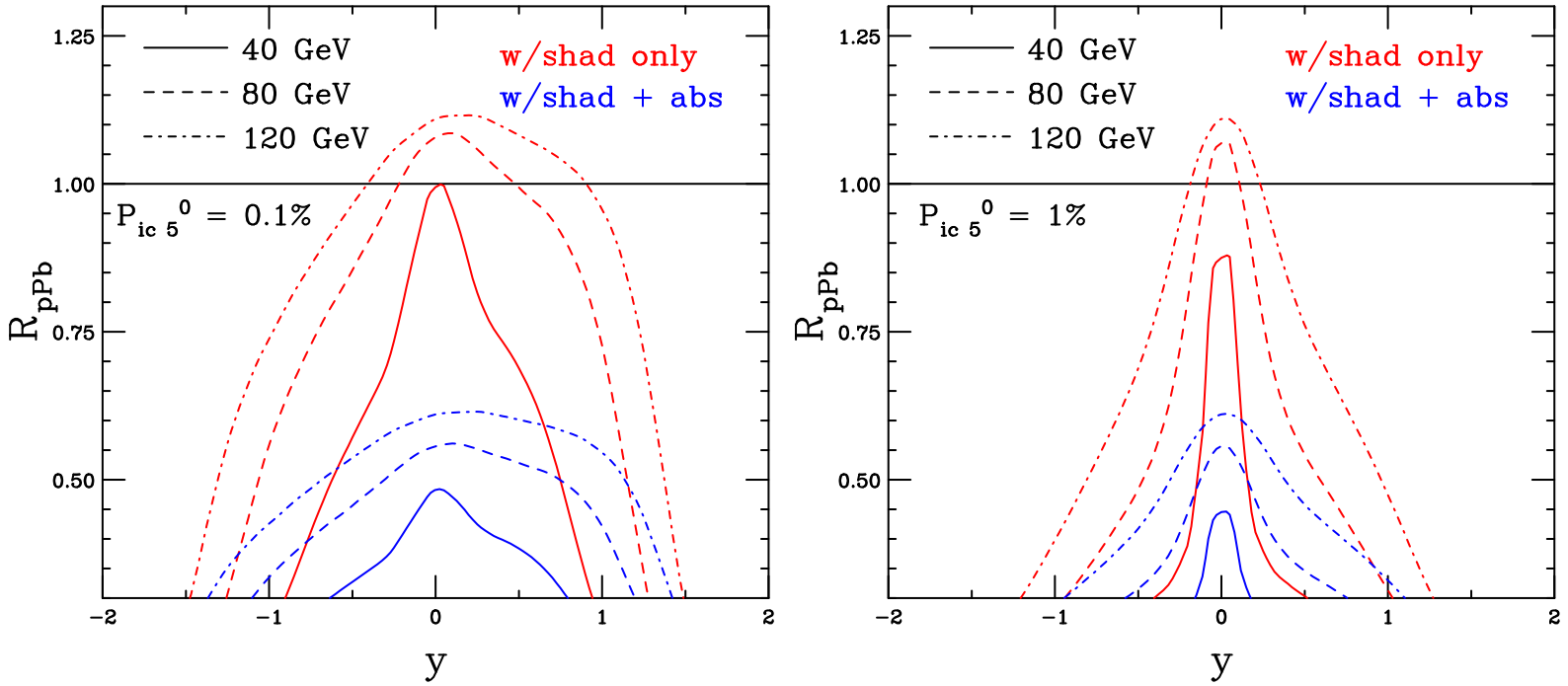

Figure 20: The nuclear modification factors for J/ψ production as a function of y for lead targets relative to proton with $P^0_{\mathrm{ic}\,5} = 0.1\%$ (left) and 1% (right). The solid, dashed and dot-dashed curves are for $p_{\mathrm{lab}} = 40$, 80 and 120 GeV respectively. The red curves are for nPDF effects alone on the pQCD contribution while the blue dashed curves include absorption on the pQCD component. Note that the rapidity distributions do not depend on the k_T broadening.

$R_{p\mathrm{Pb}}$ as a function of p_T: With Intrinsic Charm

Upper curves do not include absorption, lower curves employ $\sigma_{\mathrm{abs}} = 9$, 10 and 11 mb for $p_{\mathrm{lab}} = 120$, 80 and 40 GeV respectively

The intrinsic charm contribution is integrated over all rapidity, if it was restricted to midrapidity, $0 < y < 1$ for example, the p_T dependence would be reduced, only contributing at higher p_T

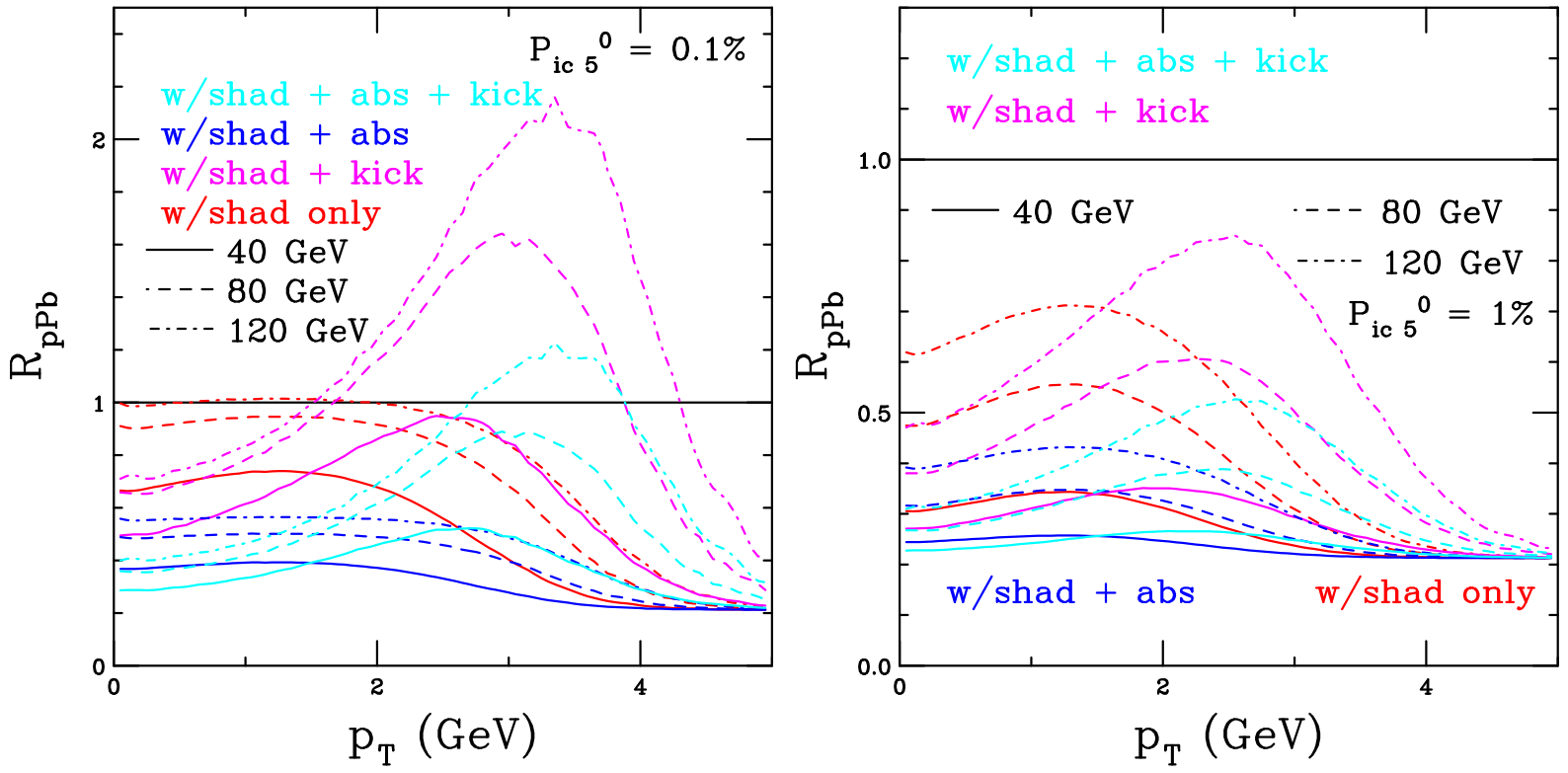

Figure 21: The nuclear modification factors for J/ψ production as a function of p_T for lead targets relative to proton with $P^0_{\mathrm{ic}\,5} = 0.1\%$ (left) and 1% (right). The solid, dashed and dot-dashed curves are for $p_{\mathrm{lab}} = 40$, 80 and 120 GeV respectively. The curves are for nPDF effects alone (red), nPDFs with an additional k_T kick (magenta), nPDFs and absorption (blue), and nPDFs, absorption and k_T broadening (cyan).

Other Potential Fixed-Target Physics Studies

.

Fixed-Target Studies for Space Radiation

Great interest in restarting space program (Artemis II and beyond, including moon bases)

Data and modeling are needed to support these missions in the areas of:

- **energy production**
- **radiation protection (dose and shielding for humans, electronics, spacecraft)**
- **nuclear propulsion**
- **planetary exploration and settlement**

Near Earth, bombardment is mostly protons up to a few hundred MeV

Further away, Galactic Cosmic Rays of protons up iron at energies from MeV to TeV scales can interact with matter

Radiation Damage to Spacecraft, Electronics & Astronauts

Solar arrays can lose power due to radiation damage

Spacecraft components can become radioactive

Single event upsets in electronics can cause temporary or permanent damage

Fission can be induced by high energy cosmic rays that penetrate shielding in reactor powered spacecraft or bases

Astronauts spending long periods in space can receive much higher doses of radiation than we do on Earth thanks to the protection of the atmosphere, potentially increasing cancer risk

Nuclear Data for Space Radiation at the EIC

Nuclear data (cross sections, multiplicities, angular distributions) are already very important for the EIC: experiment design, material budget, tracking, energy loss, energy resolution, position resolution, and many more)

Nuclear data underlie all commonly used packages (Geant, FLUKA, and others)

There are very few high energy data relevant for space physics, there is a need for beam energies up to 50 GeV/nucleon and projectiles and targets such as C, O, Al, and Fe

STAR was set up to take some of these data but RHIC shut down before it could be done

RHIC also ran U beams so the EIC could also potential study fission at the GeV scale

Fission Studies have also been Proposed for EIC

Photons can excite the nuclear beam, leading to fission (top) or resonance excitation and particle emission (arXiv:2602.17860)

Does this make any sense? Yes! There are already data to show it works.

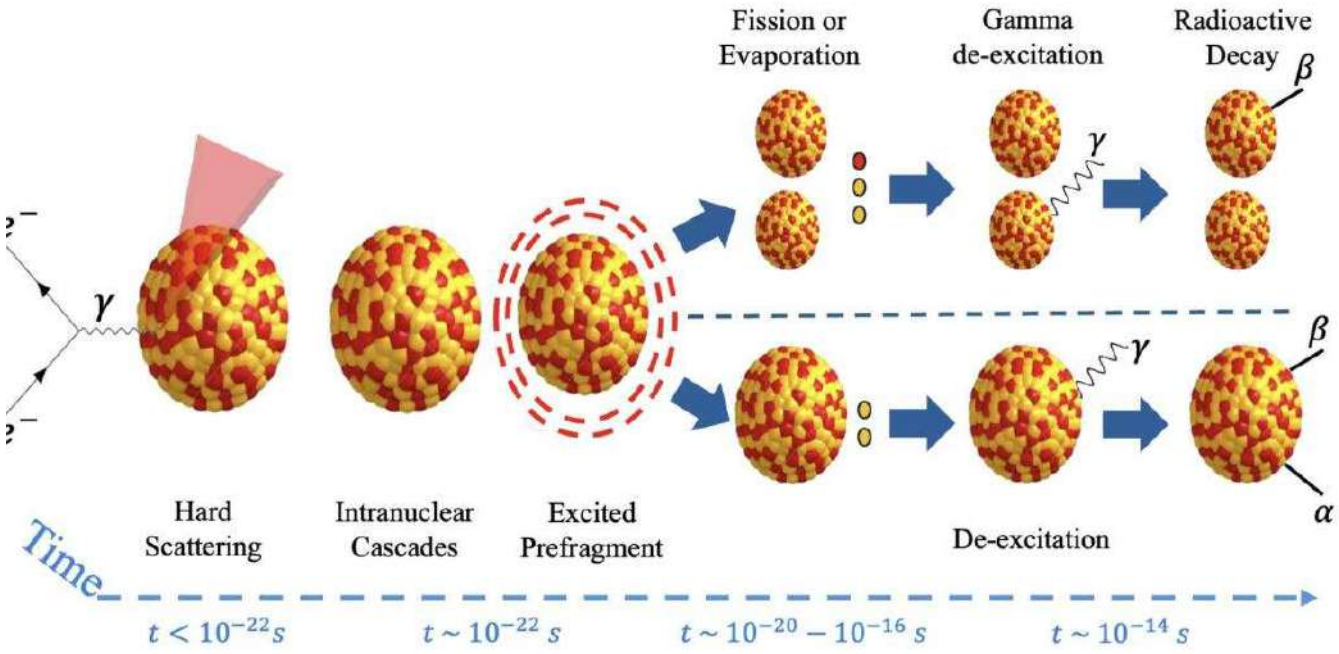

Photofission Induced by Electron Beams at JLab

JLab studied photofission of ^{237}Np, ^{233,235,238}U, ^{232}Th, and $^{\mathrm{nat}}$Pb for $0.17 < E_\gamma < 3.84$ **GeV (PRC 65, 044622 (2002)) – the peak is due to Δ baryon excitation**

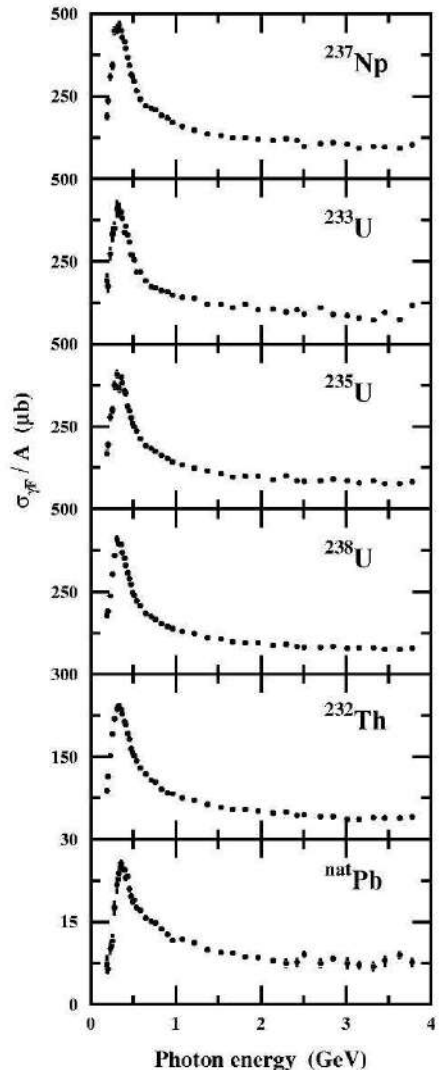

NA50 Observed Fission of Pb in Pb+Pb Collisions

The NA50 Collaboration first measured fission of ^{208}Pb with a 158 GeV Pb beam (PRC 59, 876 (1999))

Left peak – total nuclear breakup; right peak – projectile does not interact, at most a few neutrons are ejected; center peak – symmetric fission of ^{208}Pb

Top – light output of ZDC; bottom – conversion to effective charge

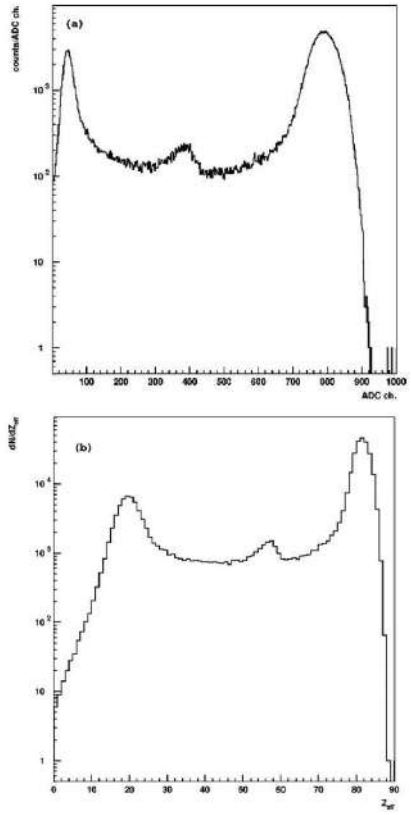

Fission Cross Section as a Function of A and E_{beam}

The NA50 Collaboration measured UPC fission of ^{208}Pb in 40 and 158 GeV Pb beams on a range of targets (PRC 59, 876 (1999) and PRC 69, 034904 (2004))

Coulomb cross section (UPCs, based on JLab measurement) proportional to Z^2; nuclear cross section (based on edge collisions of nuclei) stays constant

They saw a strong increase of the electromagnetic (UPC) fission cross section with target charge (300 mb for a Pb target)

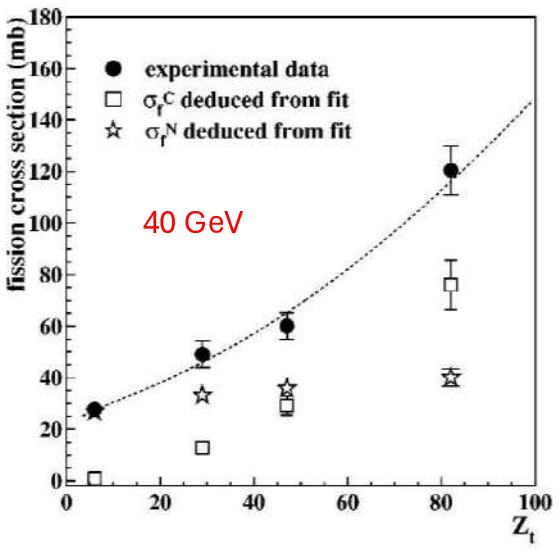

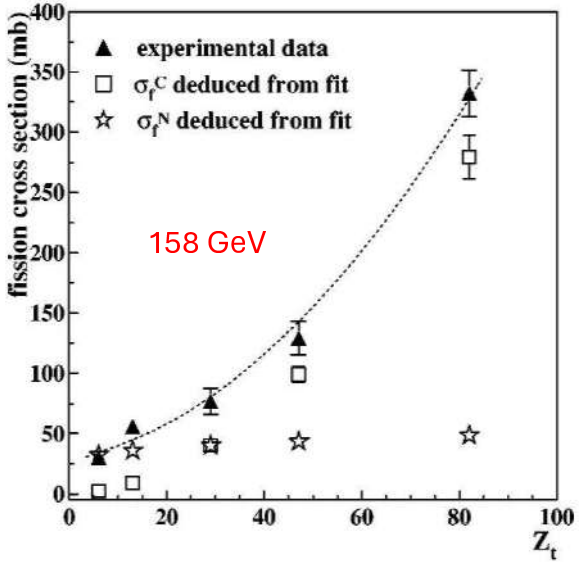

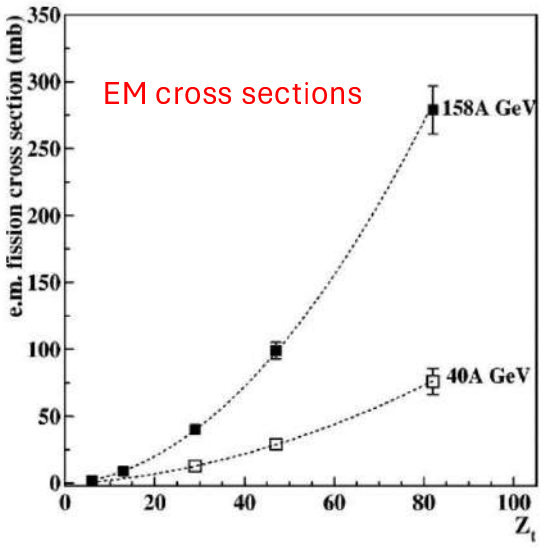

Challenges in Disentangling CNM Effects

Difficult to interpret multiple effects

Need to isolate specific effects through carefully chosen observables

Global approaches are important

Hot matter effects may play a role at collider energies

Cold QCD effects are a primary source of uncertainty in the interpretation of $A + A$ ***data***

A fixed-target program would provide added value to the EIC